Airflow distribution law of multi-branch pipe of pneumatic rice direct seeder based on dimensional analysis

Wei Qin[1,2], Zaiman Wang[1,2,3,4,5], Minghua Zhang[1,2,3,4,5], Siyu He[1,2], Xuguo Wang[1,2], Youcong Jiang[1,2], Zishun Huang[1,2], Ying Zang[1,2,3,4,5*]

(1. *Guangdong Laboratory for Lingnan Modern Agriculture, College of Engineering, South China Agricultural University, Guangzhou 510642, China*; 2. *Key Laboratory of Key Technology on Agricultural Machine and Equipment (South China Agricultural University), Ministry of Education, Guangzhou 510642, China*; 3. *Guangdong Provincial Key Laboratory of Agricultural Artificial Intelligence* (*GDKL-AAI*), *Guangzhou 510642, China*; 4. *Huangpu Innovation Research Institute of SCAU, Guangzhou 510715, China*; 5. *Maoming Branch, Guangdong Laboratory for Modern Agriculture, Maoming 525000, Guangdong, China*)

Abstract: In order to investigate the flow characteristics and distribution law of airflow in multi-branch pipe of pneumatic rice precision direct seeder and obtain the mathematical model between airflow parameters and pipe geometry structure. In this study, the airflow flow law of the multi-branch pipeline of the pneumatic system was studied, the mechanism of airflow flow in the multi-branch pipe was analyzed, and it was clarified that the main factors affecting the airflow flow in the pipe, namely, air density, air dynamic viscosity, the total flow rate of the inlet branch pipe, the length of the closed end of the header, the inner diameter of the outlet branch pipe, and the outlet branch pipe spacing. Numerical simulations were carried out using Fluent simulation software to elucidate the cause of multi-branch pipes of uneven distribution of airflow in multi-branch pipes, the empirical equation among these factors and the flow velocity of the outlet branch pipe are established by dimensional analysis method. The bench test results show that the established empirical equations are applicable in the following ranges: 0.018 $m^3/s \le Q \le 0.054$ m^3/s, 0.045 m$\le d \le$0.05 m, 0.075 m$\le L \le$0.125 m, 0.7 m$\le Y_1 \le$0.875 m (0.5 m$\le Y_2 \le$0.75 m, 0.36 m$\le Y_3 \le$0.45 m), the prediction accuracy can be controlled within 10% of the empirical formula, which can provide a reference for the prediction and optimization design of outlet velocity of the multi-branch pipe.

Keywords: pneumatic system, multi-branch pipe, axial momentum conservation, Fluent, dimensional analysis

DOI: 10.25165/j.ijabe.20231601.7663

Citation: Qin W, Wang Z M, Zhang M H, He S Y, Wang X G, Jiang Y C, et al. Airflow distribution law of multi-branch pipe of pneumatic rice direct seeder based on dimensional analysis. Int J Agric & Biol Eng, 2023; 16(1): 111–127.

1 Introduction

Pipeline is an effective carrier of fluid transmission and has wide application in the petroleum energy chemical industry[1,2], built environment engineering[3], biomedicine engineering[4], mechanical engineering[5,6], and other fields. As an important element for seeder to realize multi-row operation with one apparatus, multi-branch pipe has received wide attention from scholars in the field of agricultural engineering in terms of its operational performance and economic applicability in conveying fluids[7-10]. In the process of modern agricultural production, mechanized sowing is an important means of implementing large-scale crop production, and the high sowing quality of the seed metering mechanism is a general expectation of producers; with the in-depth research of the pneumatic seeder and the continuous optimization and improvement of its operating performance, the multi-branch pipe has become the main functional component for the pneumatic seed metering device to complete the sowing operation due to its superior air conveying performance and has been popularized and applied in the sowing process of crops such as vegetables[11], maize[12], and rice[13-16].

Currently, researchers have studied the distribution of fluids and operational efficiency in multi-branch pipes mainly from the perspective of structural optimization. Hassan et al.[17] carried out a study of the distribution of air within a five-branch line with axial inlet airflow, pointing out the effect of the ratio of the total branch area to the cross-sectional area of the manifold on the distribution of flow in the outlet branch pipe. Jimmy et al.[18] used numerical simulations to analyze the distribution of air within the branch pipes under different conditions such as non-linear variable section header and axial header air inlet angle, showing that changing the header geometry can improve the uniformity of flow distribution in each branch pipe to a certain extent. Yin et al.[12] designed a low-loss air allotter mechanism for cylindrical end cloth based on multiple branch outlets and optimized its structure to reduce fan energy losses and improve seeding consistency during maize seeding operations. Shu et al.[19] developed a fan selection model and a model of the relationship between the negative pressure of the seed metering device and the number of seed metering devices, the rated power of the fan, and the operating speed of the fan based on multi-branch piping, which provided a basis for the design of the seed metering mechanism for rapeseed. Song et al.[2] used

Received date: 2022-05-07 **Accepted date:** 2022-10-18

Biographies: Wei Qin, PhD candidate, research interest: agricultural mechanization and automation, Email: 1240672079@qq.com; **Zaiman Wang**, Associate Professor, research interest: agricultural mechanization and automation, Email: wangzaiman@scau.edu.cn; **Minghua Zhang**, Lecturer, research interest: agricultural mechanization and automation, Email: zhangminghuascau@163.com; **Siyu He**, PhD candidate, research interest: agricultural mechanization and automation, Email: 1141903213@qq.com; **Xuguo Wang**, MS candidate, research interest: agricultural mechanization and automation, Email: 1044398570@qq.com; **Youcong Jiang**, MS candidate, research interest: agricultural mechanization and automation, Email: 794602322@qq.com; **Zishun Huang**, MS candidate, research interest: agricultural mechanization and automation, Email: 375529755@qq.com.

***Corresponding author: Ying Zang**, PhD, Professor, research interest: agricultural mechanization and automation. College of Engineering, South China Agricultural University, Guangzhou 510642, China. Tel: +86-20-38676975, Email: yingzang@scau.edu.cn.

numerical simulations to analyze the flow law of the internal fluid in the pipeline with axially inlet inclined branch pipe, header variable section pipe, and the different branch-to-header cross-sectional area ratios, and proposed a critical condition to avoid vortex flow in the branch inlet of the multi-branch pipe. Qin et al.[20] used numerical simulation to study the flow distribution and pressure loss of multi-branch pipes with axial inlets and gave a numerical model for a reasonable study of multi-branch pipes.

In summary, researchers have conducted more research on air flow in multi-branch pipes with the help of numerical simulation methods, and it is clear that the geometric structure of multi-branch pipes is the main factor affecting the flow and distribution of pipe airflow, although there is some progress in related research, few papers have provided guidance on the initial design process of multi-branch pipes, and there is no relevant empirical model to predict the airflow parameters of multi-branch pipes with continuous tee structure. Especially in the field of agricultural engineering, due to the need for agronomic integration of crops, researchers often focus more on the performance improvement of seed metering device operating units when designing pneumatic pipes for seeder, and there is no unified and relatively universal empirical formula for pipe selection, and the pipe design process is rarely mentioned. In this study, based on the multi-branch pipe of pneumatic rice precision direct seeder, we analyzed the flow mechanism of multi-branch pipe of pneumatic system of rice precision direct seeder, established the mathematical model of geometric structure of multi-branch pipe, determined the main experimental factors affecting the flow of air, combined with the method of dimensional analysis, and studied the outlet branch pipe of multi-branch pipe under the influence of different experimental factors with the help of computational fluid dynamics software Fluent and full-size model test. The empirical formula for predicting the airflow parameters of each outlet branch pipe of multi-branch pipe is established to provide reference for the design selection and structure optimization of multi-branch pipe of pneumatic system.

2 Experiment materials

2.1 Test bench

The full-scale model test bench for a multi-branch pipeline as shown in Figure 1a, is mainly composed of a fan (power 2.2 kW, maximum air volume 260 m^3/h), velocity control inverter (power 2.2 kW), Anemometer (range 0-60 m/s), multi-branch pipe, and other parts, the whole test bench is fixed on the frame constructed by industrial aluminum profiles (40 mm×40 mm). The multi-branch pipe's installation layout is referred to as the pneumatic rice precision hole direct seeder[34], and each pipe component of the multi-branch pipe is processed by 3D printing (9400 resin material).

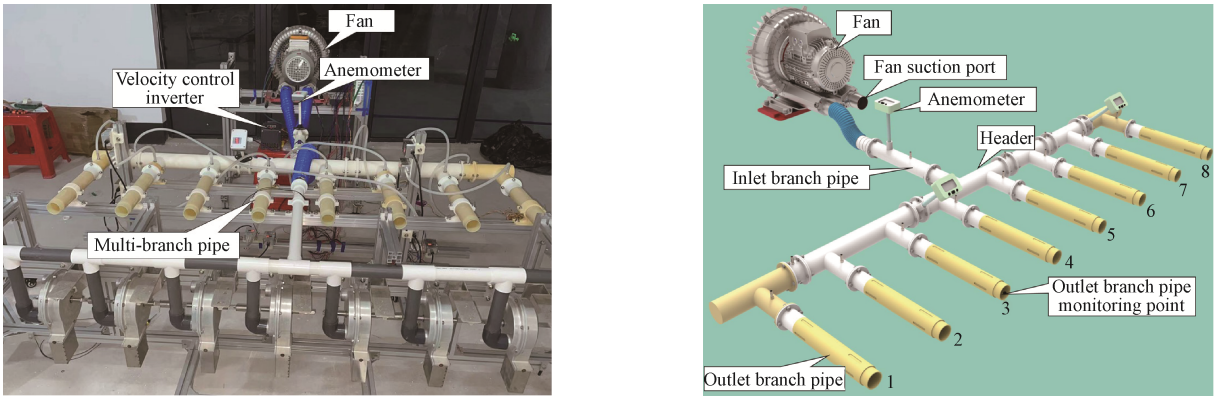

a. Test bench b. Multi-branch pipe structure diagram

Figure 1 Multi-branch piping full-size test bench

As shown in Figure 1b, the multi-branch pipe consists of an inlet branch pipe, a header, and eight outlet branch pipes, of which the inlet branch pipe is located in the middle of the header, and the outlet branch pipes are symmetrically distributed at equal intervals along both sides of the header pipe axially with the inlet branch pipe as the middle, and the length of the inner diameter of each outlet branch pipe is equal. During its operation, the airflow enters the header through the inlet branch pipe, and then the header divides into the outlet branch pipe to achieve the distribution of airflow. The initial dimensions of the multi-branch pipe are the length of the inlet branch pipe is 0.24 m, the inner diameter of the inlet branch pipe is 0.048 m; the inner diameter of the header is 0.06 m, the length of the closed end of the header is 0.075 m, the length of the outlet branch pipe is 0.36 m, the inner diameter of the outlet branch pipe is 0.045 m.

2.2 Gas flow principle of multi-branch pipe

The tee is the main fitting of the multi-branch pipe, which enables the air in the pipe to be diverted and is an important component for transporting the air to the specific operating position of the seed metering mechanism. In this paper, the tee at the junction of the header and the branch pipe is used as the basic analysis element to analyze the trend of the air movement in the header and the outlet branch pipe. Figure 2 shows the flow of air from the inlet branch pipe tee through the header tee into the outlet branch pipes 1 to 4. Figures 3a and 3b show the local flow of air in the inlet branch section and the local tee represented near the junction of the header and branch pipe, respectively. Figure 3a shows the flow distribution after the air enters the header via the inlet branch pipe. a is the airflow control volume at this point, assuming equal flow rates Q_1 and Q_2 on both sides of the header, with Q_1 being the flow rate into the left header. Figure 3b shows the distribution of air near a section of the header tee, in the air control volume b, ignoring the pressure loss due to friction; at this point, a portion of the air flows into the outlet branch pipe at a normal velocity V_{iy} due to the differential pressure between the header and the ambient, the loss of fluid will cause the flow to decelerate, which in turn will cause $P_{i-1}>P_i$; the other part continues to flow along the header tube to the next tee under the dual action of air inertia and the pressure difference between the two sides of the control volume, where the momentum of the control volume b in the axial direction satisfies the following equation[31]:

$$\int P_i \mathrm{d}A - \int P_{i-1} \mathrm{d}A = \int \rho V_{i-1}^2 \mathrm{d}A - \int \rho V_i^2 \mathrm{d}A + \int \rho V_{ix} V_{iy} \mathrm{d}A_j \quad (1)$$

where, j is the serial number of the outlet branch pipe, j=1, 2, 3, 4, the same below; P_i is the static pressure of air into the control volume, Pa, i=j, the same below; V_i is the velocity of the air into the control volume, m/s; P_{i-1} is the static pressure of the air out of the control volume, Pa; V_{i-1} is the velocity of the air out of the control volume, m/s; V_{ix} is the axial velocity component of the air into the outlet branch pipe, m/s; V_{iy} is the normal velocity component of the airflow into the outlet branch pipe, m/s; ρ is the density of the air in the outlet branch pipe, kg/m^3; A is the area of the header, m^2; A_j is the area of the outlet branch pipe, m^2.

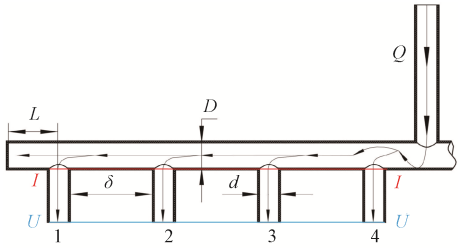

Note: Q is the total flow rate of the inlet branch pipe, m^3/s; D is the inner diameter of the header pipe, mm; L is the length of the closed end of the header pipe, mm; δ is the outlet branch pipe spacing, mm; d is the inner diameter of the outlet branch pipes, mm.

Figure 2 Flow principle diagram of multi-branch pipe

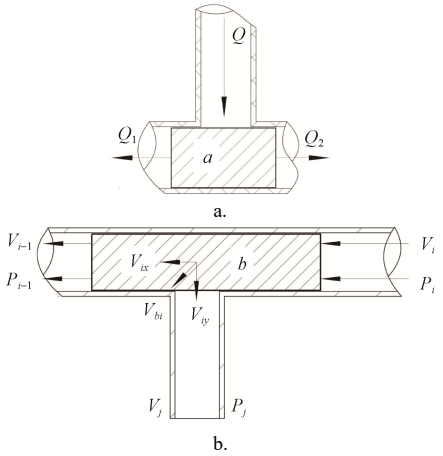

Figure 3 Flow principle diagram of local tee in the multi-branch pipe

Assuming that the values in the integrals $\int P_i \mathrm{d}A$, $\int P_{i-1} \mathrm{d}A$, $\int \rho V_i^2 \mathrm{d}A$, and $\int \rho V_{i-1}^2 \mathrm{d}A$ are all average values, if there is no axial momentum loss when the airflow exits the control volume b, which is contrary to the reality that the airflow enters the outlet branch pipe and is diverted, and therefore V_i>V_{ix}; since the uncertainty of the axial momentum transmission of the flow to the outlet branch pipe, the value of the integral $\int \rho V_{ix} V_{iy} \mathrm{d}A_j$ will normally be determined according to the actual test, and from the perspective of continuity, it is assumed that the value of V_{iy} is equal to the velocity value just entering the I-I boundary, and the equation of motion of the fluid flowing into the I-I boundary is controlled by Bernoulli's equation, thus the equation of airflow flows into the outlet branch pipe can be obtained as:

$$P_{iy} + \frac{1}{2}\rho V_{iy}^2 = P_j + \frac{1}{2}\rho V_j^2 + H_j \quad (2)$$

where, P_{iy} is the static pressure of the air at the I-I boundary of outlet branch pipe 1-4, Pa; V_{iy} is the velocity of the air at the I-I boundary of outlet branch pipe 1-4, m/s; P_j is the static pressure of the air at the U-U boundary of outlet branch pipe 1-4, Pa; V_j is the velocity of the air at the U-U boundary of outlet branch pipe 1-4, m/s; H_j is the drag loss in the outlet branch pipe 1-4 (including local loss and along the way loss), Pa.

2.3 Mathematical model establishment

To determine the relationship between the airflow parameters of each outlet branch pipe in the multi-branch pipe and the parameters of the pipe geometry mechanism, the center point of the inlet branch pipe is taken as the origin, the direction of the airflow inlet is the x-axis, and the direction perpendicular to the airflow inlet is the y-axis, and the Cartesian coordinate system between the monitoring points of the inlet branch pipe and the outlet branch pipe is established, as shown in Figure 4. The length of the monitoring point of the outlet branch pipe section is l_0 (m), and the three points A, B, and C represent the three monitoring points of outlet branch pipes 1, 2, and 3. As can be seen from Figure 4, the length of the ON is the horizontal coordinate of the three points A, B, and C. The value of the vertical coordinate is related to the distance δ (m) between the outlet branch pipes, from which the relationship between the coordinates of the points can be obtained as follows:

$$\begin{cases} x_j = l + D + l_0 \\ y_j = \left(\dfrac{9}{2} - j\right)\delta \end{cases} \quad (3)$$

where, j is the serial number of the outlet branch pipe; l is the length of the inlet branch pipe, mm.

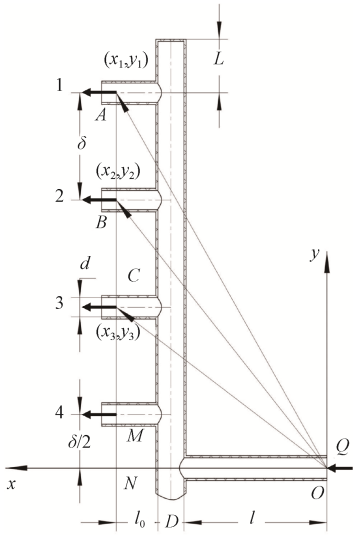

Figure 4 Cartesian coordinate system of the multi-branch pipe

From Equation (3), it can be seen that the variation of the monitoring point at x_j depends on the variation of the l-value, d-value, and the monitoring point length l_0-value. To make the air flow evenly at the monitoring point of the outlet branch pipe, the monitoring point is set at a distance of 5 times the inner diameter of the outlet branch pipe to obtain a more stable velocity value, so l_0 = 5d. Therefore, the change of d will directly affect the value of x_j, and the change of the value of j will not change the specific value of x_j. For the outlet branch pipes of the same inner diameter, the value of x_j is fixed. Combined with Equation (3), the change of the monitoring point at y_j mainly depends on the distance δ between adjacent outlet branch pipes and the change of the value of j at the position of the outlet branch pipe, both of which determine the value of y_j.

In summary, let X= x_j, Y= y_j, and further summary show that

the horizontal coordinate value X (m) of the outlet branch pipe monitoring point, the length L (m) of the closed end of the header, the vertical coordinate value Y (m) of the outlet branch pipe monitoring point and the inner diameter d (m) of the outlet branch pipe are the main geometric structure factors affecting the outlet parameters of each branch pipe.

3 Research method

The research on multi-branch pipes is carried out by a combination of numerical simulation and model experiments. Numerical simulation experiments have a short research period and low cost and have been widely used in pipe fluid analysis, and the effectiveness of their simulation results has also been recognized by researchers in related fields[2,19]. Therefore, this study investigates the flow pattern and decay mechanism of airflow in the multi-branch pipe through CFD simulation and obtains high accuracy test data through a full-size model experiment.

3.1 Numerical simulation methodology

The research shows that the pressure at the measurement points of the mutually symmetrical outlet branch pipes is approximately symmetrically equal when the inlet branch pipe is in the middle position[32,33]. Therefore, before investigating the mechanism of air in a multi-branch pipe, the following assumptions are made about the air in the pipe: 1) The working fluid in the multi-branch pipe is only air (25°C), with a stable density, which can be regarded as an incompressible fluid; ignore the mass of the air and assume that it flows isothermally along a uniform cross-section in the pipe, disregarding the effect of temperature changes on energy loss. 2) The air in the pipe is in a constant flow and a turbulent state, the measured air pressure and the velocity of the air are the averages of the data from the monitoring points. 3) Neglecting the influence of the wall roughness of the multi-branch pipe on the airflow in the pipe, the flow rate from the inlet branch pipe of the multi-branch pipe to both sides of the header is equal. According to the above assumptions, combined with the relevant knowledge of fluid mechanics, the mass continuity conservation equation and the momentum conservation equation of air can be found as follows[14]:

$$\begin{cases} \dfrac{\partial u}{\partial x}+\dfrac{\partial v}{\partial y}+\dfrac{\partial w}{\partial z}=0 \\ \dfrac{\partial(\rho uu)}{\partial \mathrm{x}}+\dfrac{\partial(\rho vu)}{\partial z}+\dfrac{\partial(\rho wu)}{\partial z}=\dfrac{\partial}{\partial x}\left(\mu_{eff}\dfrac{\partial u}{\partial x}\right)+ \\ \quad \dfrac{\partial}{\partial y}\left(\mu_{eff}\dfrac{\partial u}{\partial y}\right)+\dfrac{\partial}{\partial z}\left(\mu_{eff}\dfrac{\partial u}{\partial z}\right)-\dfrac{\partial p}{\partial x}+S_u \\ \dfrac{\partial(\rho uv)}{\partial \mathrm{x}}+\dfrac{\partial(\rho vv)}{\partial z}+\dfrac{\partial(\rho wv)}{\partial z}=\dfrac{\partial}{\partial x}\left(\mu_{eff}\dfrac{\partial v}{\partial x}\right)+ \\ \quad \dfrac{\partial}{\partial y}\left(\mu_{eff}\dfrac{\partial v}{\partial y}\right)+\dfrac{\partial}{\partial z}\left(\mu_{eff}\dfrac{\partial v}{\partial z}\right)-\dfrac{\partial p}{\partial y}+S_v \\ \dfrac{\partial(\rho uu)}{\partial \mathrm{x}}+\dfrac{\partial(\rho vu)}{\partial z}+\dfrac{\partial(\rho wu)}{\partial z}=\dfrac{\partial}{\partial x}\left(\mu_{eff}\dfrac{\partial w}{\partial x}\right)+ \\ \quad \dfrac{\partial}{\partial y}\left(\mu_{eff}\dfrac{\partial w}{\partial y}\right)+\dfrac{\partial}{\partial z}\left(\mu_{eff}\dfrac{\partial w}{\partial z}\right)-\dfrac{\partial p}{\partial z}+S_w \end{cases} \tag{4}$$

where, u, v, and w are the velocity components in the x, y, and z axes of space respectively, m/s; ρ is the fluid dynamic density, kg/m^3; μ_{eff} is the effective viscosity coefficient, which is related to the fluid dynamic viscosity μ, Pa·s; p is isotropic pressure, N; S_u, S_v, and S_w are the generalized source term of the momentum conservation equation when the mass force only considers gravity, $S_u = S_v = 0$, $S_w = -\rho g$.

It can be seen from Equations (4) and (5) that ρ and μ are also a factor that affects the flow velocity at the outlet of each branch pipe.

3.1.1 Setting of simulation experiment parameters

To describe the airflow characteristics in multi-branch pipe air flow at the microscale, a multi-branch pipe geometric model was constructed based on Ansys Fluent software, and due to the complex flow trend of the air at the junction of the header and the outlet branch pipe, mesh refinement was carried out at the adjacent area of the junction of the outlet branch pipe and the header of the multi-branch pipe, as shown in Figure 5, when the number of meshes was 470 000, the simulation results had no significant effect on the average flow velocity at the outlet branch pipe, the Realizable k-ε turbulence model was determined as the simulation experiment model by combining the references[2,19]. At the dividing flow type of header structure in the multi-branch pipe, the dramatically changing pressure gradient also causes the boundary layer to separate, so the enhanced wall treatment is used near the wall, the spatial discrete and coupled solution method of pressure and velocity adopts SIMPLE algorithm, the equation discretization iterations are all in second-order windward format, the convergence stubble of each iteration variable is set to 0.001 and the number of iteration steps is 1000. The inlet boundary is set to the average flow velocity and the outlet boundary is set to the pressure, and the outlet gauge pressure is set to 0 for comparative analysis of the simulation results.

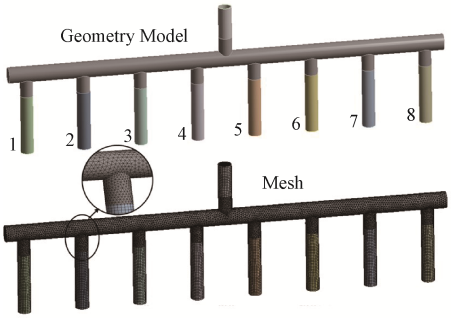

Figure 5 Simulation model of multi-branch pipe

3.1.2 Design of simulation experiment

According to the above analysis, the main factors affecting the flow velocity v_n of each branch pipe of the multi-branch pipe include: ρ, μ, Q, X, L, Y, and d. Where ρ, μ, and X are constant values and Y is determined by the outlet branch pipe spacing δ. Therefore, based on the initial size of the multi-branch pipe, taking the total flow rate Q of the inlet branch pipe, the inner diameter d of the outlet branch pipe, the length L of the closed end of the header, and the outlet branch pipe spacing δ as the experimental factors, a single-factor experimental design was carried out, and five levels were selected for each experiment factor. The selection of the Q level was determined in accordance with the value of fan flow corresponding to the operation of the pneumatic rice precision hole direct seeder[32,34], and the selection of the d level was determined based on the value of positive and negative pressure outlet inner diameter of each type of pneumatic seed metering device previously tried and tested by the team[32,34], the selection of L value was determined with reference [20], and the selection of δ level was determined based on the agronomic requirements of rice sowing row spacing, and the experimental scheme is listed in Table 1.

Table 1 Design of simulation experiment scheme

Level	Factors			
	Q/ m^3·s^{-1}	d/ m	L/ m	δ/ m
1	0.018	0.020	0.025	0.200
2	0.027	0.025	0.050	0.225
3	0.036	0.030	0.075	0.250
4	0.045	0.045	0.100	0.275
5	0.054	0.050	0.125	0.300

Let P_{in} be the total pressure at the outlet branch pipe *I-I* boundary and P_{out} be the total pressure at the *U-U* boundary, which can be deduced from Equation (2):

$$\begin{cases} P_{out} = P_{in} - H_j \\ P_{in} = P_{iy} + \dfrac{1}{2}\rho V_{iy}^2 \\ P_{out} = P_j + \dfrac{1}{2}\rho V_j^2 \end{cases} \tag{5}$$

According to the setting of simulated outlet conditions, the P_j value of each outlet branch pipe is equal, so the P_{out} value is determined by the air velocity at the outlet branch pipe. The dimensionless parameter is used as the consistency evaluation index of P_{in} value at the inlet of each outlet branch pipe and P_{out} value at the outlet in the simulation experiment, and its calculation formula is,

$$\begin{cases} \Phi_{ky} = \dfrac{P_{in}}{\overline{P_{in}}} \\ \Phi_k = \dfrac{P_{out}}{\overline{P_{out}}} \end{cases} \tag{6}$$

where, Φ_{ky} and Φ_k are the consistency evaluation indexes for the inlet P_{in} and outlet P_{out} value of the *I-I* boundary and *U-U* boundary of the outlet branch pipe respectively, and k=1, 2, 3, 4; the superscript "-" indicates the average value of the total pressure at the inlet and outlet of each branch pipe.

3.2 Full-scale model test

3.2.1 The established Π equation

The dimensional analysis method is a relatively accurate and fast method of establishing the functional relationship between multiple experimental factors and experimental indexes[25,26]. It can combine many factors into an empirical formula with a more accurate scope of application and can predict the relevant solution parameters.

Based on the experimental factors mentioned above and the Π theorem modified by Jiang et al.[21-23], eight variables are determined, which are v_n, ρ, X, μ, Q, d, L, and Y. This problem is an engineering problem of applied research, therefore, the *MLT* system is chosen as the dimensional analysis system, with the mass dimension M, length dimension L, and time dimension T as the basic dimensions, and the rest of the dimensions as the derived dimensions to be obtained by the experimental factors and dimensions as listed in Table 2.

Table 2 Experimental factors and dimensions

Item		Factors symbol							
		ρ	X	μ	Q	d	L	Y	v_n
Units		kg·m^{-3}	m	Pa·s	m^3·s^{-1}	m	m	m	m·s^{-1}
Dimension		ML^{-3}	L	$ML^{-1}T^{-1}$	L^3T^{-1}	L	L	L	LT^{-1}
Matrix coefficient		α_1	α_2	α_3	α_4	α_5	α_6	α_7	α_8
Dimensional matrix coefficient	M	1	0	1	0	0	0	0	0
	L	–3	1	–1	3	1	1	1	1
	T	0	0	–1	–1	0	0	0	–1
Relational matrix coefficient	Π_1	1	–1	–1	1	0	0	0	0
	Π_2	0	–1	0	0	1	0	0	0
	Π_3	0	–1	0	0	0	1	0	0
	Π_4	0	–1	0	0	0	0	1	0
	Π_5	1	1	–1	0	0	0	0	1

Based on the Π theorem and the Π relational matrix coefficients in Table 2, the five similarity criteria shown in Equation (7) are obtained, namely

$$\Pi_1 = v_n\rho X/\mu, \Pi_2 = \rho Q/X\mu, \Pi_3 = d/X, \Pi_4 = L/X, \Pi_5 = Y/X \tag{7}$$

Taking the Π_1 item containing the flow velocity v_n of the outlet branch pipe as the dependent variable, the following functional relationship can be obtained according to Jiang's theorem:

$$\begin{cases} \Pi_1 = f\left(\Pi_2, \Pi_3, \Pi_4, \Pi_5\right) \\ \dfrac{v_n\rho X}{\mu} = f\left(\dfrac{\rho Q}{X\mu}, \dfrac{d}{X}, \dfrac{L}{X}, \dfrac{Y}{X}\right) \end{cases} \tag{8}$$

3.2.2 Design of the full-scale model

The values of the variables ρ and μ were fixed throughout the experiment, while it is clear from Equation (6) that a change in the value of X value will affect the change in each Π item, therefore, the value of X must be fixed, as well as the values of the parameters value l, D, and l_0 value must also be fixed that determine the value of X; the design of the experimental scheme was carried on this basis.

1) Design of $\left(\Pi_{1/2}\right)_{\bar{3},\bar{4},\bar{5}}$ and $\left(\Pi_{1/2}\right)_{\bar{3},\bar{4},\bar{5}}$

In this part, the effect of a change in the independent variable Π_2 on the dependent variable Π_1 was discussed, Since the values ρ, μ, and X was fixed, Π_2 would vary with Q, meanwhile, the values of Π_3, Π_4, Π_5 (represented by $\Pi_{\bar{3}}$, $\Pi_{\bar{4}}$, $\Pi_{\bar{5}}$ respectively, the same as below) were fixed, the base value of Q was set to 0.018 m^3/s, each level increased by 0.009 m^3/s until it increases to 0.054 m^3/s.

Design of $\Pi_{\bar{3}}$: Because X was fixed, the variable $\Pi_{\bar{3}}$ would vary with d, d was set to 0.045 m and X was 0.6 m, then $\Pi_{\bar{3}}$=0.075.

Design of $\Pi_{\bar{4}}$: Because X was fixed, the variable $\Pi_{\bar{4}}$ would vary with L, L was set to 0.075 m and X was 0.6 m, then $\Pi_{\bar{4}}$=0.125.

Design of $\Pi_{\bar{5}}$: Because X was fixed, the variable $\Pi_{\bar{5}}$ would vary with Y_1, Y_1 was set to 0.875 m and X was 0.6 m, then $\Pi_{\bar{5}}$=1.46.

To confirm the effectiveness of the combination equation, it was necessary to set one of $\Pi_{\bar{3}}$, $\Pi_{\bar{4}}$, $\Pi_{\bar{5}}$ to be another fixed value. Here, Y_1 was set to 1.05 m, then $\Pi_{\bar{5}}^{=}$=1.75. The experimental scheme is listed in Table 3 (Note: the design values of the corresponding parameters $\Pi_{\bar{5}}$ and $\Pi_{\bar{5}}^{=}$ of the outlet branch

pipes 2 and 3 are listed in Table 3).

2) Design of $\left(\Pi_{1/3}\right)_{\bar{2},\bar{4},\bar{5}}$ and $\left(\Pi_{1/3}\right)_{\bar{2},\bar{4},\bar{\bar{5}}}$

In this part, the effect of a change in the independent variable Π_3 on the dependent variable Π_1 was discussed, because the value of X was fixed, therefore, the Π_3 was varied with the inner diameter d of the outlet branch pipe; meanwhile, the values of Π_2, Π_4, and Π_5 were fixed, the base value of d was set to 0.02 m, and according to the inner diameter value of the airflow chamber of the seed metering device designed by the team in the early stage, the remaining d values were determined, which were 0.025 m, 0.03 m, 0.045 m, 0.05 m, respectively.

Table 3 Experimental design of Π equations of $\left(\Pi_{1/2}\right)_{\bar{3},\bar{4},\bar{5}}$ and $\left(\Pi_{1/2}\right)_{\bar{3},\bar{4},\bar{\bar{5}}}$

No.	ρ/kg·m^{-3}	X/m	μ/Pa·s	Q/m^3·s^{-1}	d/m	L/m	Y_1/m	Y_2/m	Y_3/m
1	1.17	0.6	1.84×10^{-5}	**0.018**	0.045	0.075	0.875(**1.05**)	0.625(**0.75**)	0.375(**0.45**)
2	1.17	0.6	1.84×10^{-5}	**0.027**	0.045	0.075	0.875(**1.05**)	0.625(**0.75**)	0.375(**0.45**)
3	1.17	0.6	1.84×10^{-5}	**0.036**	0.045	0.075	0.875(**1.05**)	0.625(**0.75**)	0.375(**0.45**)
4	1.17	0.6	1.84×10^{-5}	**0.045**	0.045	0.075	0.875(**1.05**)	0.625(**0.75**)	0.375(**0.45**)
5	1.17	0.6	1.84×10^{-5}	**0.054**	0.045	0.075	0.875(**1.05**)	0.625(**0.75**)	0.375(**0.45**)

Note: The values in brackets are the $\left(\Pi_{1/2}\right)_{\bar{3},\bar{4},\bar{5}}$ values used in the experiment, compare with $\left(\Pi_{1/2}\right)_{\bar{3},\bar{4},\bar{\bar{5}}}$, It is only the difference in value, and the meaning shown in the following table is the same.

Design of $\Pi_{\bar{2}}$: Because the values of ρ, μ, and X were fixed, so $\Pi_{\bar{2}}$ would change with the value Q, If the Q value is set to 0.036 m^3/s, and the X value was 0.6 m, then $\Pi_{\bar{2}}$=3815.22.

Design of $\Pi_{\bar{4}}$: Because X was fixed, the variable $\Pi_{\bar{4}}$ would vary with L, L was set to 0.075 m and X was 0.6 m, then $\Pi_{\bar{4}}$=0.125.

Design of $\Pi_{\bar{5}}$: Because X was fixed, the variable $\Pi_{\bar{5}}$ would vary with Y_1, Y_1 was set to 0.875 m and X was 0.6 m, then $\Pi_{\bar{5}}$=1.46.

To confirm the effectiveness of the combination equation, Y_1 was set to 1.05 m, then $\Pi_{\bar{\bar{5}}}$=1.75. This part experimental scheme is listed in Table 4 (Note: the design values of the corresponding parameters $\Pi_{\bar{5}}$ and $\Pi_{\bar{\bar{5}}}$ of the outlet branch pipes 2 and 3 are listed in Table 4).

Table 4 Experimental design of Π equations of $\left(\Pi_{1/3}\right)_{\bar{2},\bar{4},\bar{5}}$ and $\left(\Pi_{1/3}\right)_{\bar{2},\bar{4},\bar{\bar{5}}}$

No.	ρ/kg·m^{-3}	X/m	μ/Pa·s	Q/m^3·s^{-1}	d/m	L/m	Y_1/m	Y_2/m	Y_3/m
1	1.17	0.6	1.84×10^{-5}	0.036	**0.020**	0.075	0.875(**1.05**)	0.625(**0.75**)	0.375(**0.45**)
2	1.17	0.6	1.84×10^{-5}	0.036	**0.025**	0.075	0.875(**1.05**)	0.625(**0.75**)	0.375(**0.45**)
3	1.17	0.6	1.84×10^{-5}	0.036	**0.030**	0.075	0.875(**1.05**)	0.625(**0.75**)	0.375(**0.45**)
4	1.17	0.6	1.84×10^{-5}	0.036	**0.045**	0.075	0.875(**1.05**)	0.625(**0.75**)	0.375(**0.45**)
5	1.17	0.6	1.84×10^{-5}	0.036	**0.050**	0.075	0.875(**1.05**)	0.625(**0.75**)	0.375(**0.45**)

3) Design of $\left(\Pi_{1/4}\right)_{\bar{2},\bar{3},\bar{5}}$ and $\left(\Pi_{1/4}\right)_{\bar{2},\bar{3},\bar{\bar{5}}}$

In this part, the influence of the change of the independent variable Π_4 on the dependent variable Π_1 was discussed. Because the value of X was fixed, the Π_4 was varied with the value of L; because the values of Π_2, Π_3, and Π_5 were fixed, and the base value of L was set to 0.025 m, each level increased by 0.125 m until it increases to 0.025 m.

Design of $\Pi_{\bar{2}}$: Because the values of ρ, μ, and X were fixed, so $\Pi_{\bar{2}}$ would change with the value Q, If the Q value was set to 0.036 m^3/s, and the X value was 0.6 m, then $\Pi_{\bar{2}}$=3815.22.

Design of $\Pi_{\bar{3}}$: Because X was fixed, the variable $\Pi_{\bar{3}}$ would vary with d, d was set to 0.045 m and X was 0.6 m, then $\Pi_{\bar{3}}$=0.075.

Design of $\Pi_{\bar{5}}$: Because X was fixed, the variable $\Pi_{\bar{5}}$ would vary with Y_1, Y_1 was set to 0.875 m and X was 0.6 m, then $\Pi_{\bar{5}}$=1.46.

To confirm the effectiveness of the combination equation, Y_1 was set to 1.05 m, then $\Pi_{\bar{\bar{5}}}$=1.75. This part experimental scheme is listed in Table 5 (Note: the design values of the corresponding parameters $\Pi_{\bar{5}}$ and $\Pi_{\bar{\bar{5}}}$ of the outlet branch pipes 2 and 3 are listed in Table 5).

Table 5 Experimental design of Π equations of $\left(\Pi_{1/4}\right)_{\bar{2},\bar{3},\bar{5}}$ and $\left(\Pi_{1/4}\right)_{\bar{2},\bar{3},\bar{\bar{5}}}$

No.	ρ/kg·m^{-3}	X/m	μ/Pa·s	Q/m^3·s^{-1}	d/m	L/m	Y_1/m	Y_2/m	Y_3/m
1	1.17	0.6	1.84×10^{-5}	0.036	0.045	**0.025**	0.875(**1.05**)	0.625(**0.75**)	0.375(**0.45**)
2	1.17	0.6	1.84×10^{-5}	0.036	0.045	**0.050**	0.875(**1.05**)	0.625(**0.75**)	0.375(**0.45**)
3	1.17	0.6	1.84×10^{-5}	0.036	0.045	**0.075**	0.875(**1.05**)	0.625(**0.75**)	0.375(**0.45**)
4	1.17	0.6	1.84×10^{-5}	0.036	0.045	**0.100**	0.875(**1.05**)	0.625(**0.75**)	0.375(**0.45**)
5	1.17	0.6	1.84×10^{-5}	0.036	0.045	**0.125**	0.875(**1.05**)	0.625(**0.75**)	0.375(**0.45**)

4) Design of $\left(\Pi_{1/5}\right)_{\bar{2},\bar{3},\bar{4}}$ and $\left(\Pi_{1/5}\right)_{\bar{2},\bar{3},\bar{\bar{4}}}$

In this part, the influence of the change of the independent variable Π_5 on the dependent variable Π_1 was discussed. Because the value of X was fixed, the change of Π_5 was mainly carried out by changing the value of δ; meanwhile, the values of Π_2, Π_3, and Π_4 were fixed, the base value of δ was set at 0.7 m and increased to 1.05 m in steps of 0.0875 m.

Design of $\Pi_{\bar{2}}$: Because the values of ρ, μ, and X were fixed, so $\Pi_{\bar{2}}$ would change with the value Q, If the Q value is set to 0.036 m^3/s, and the X value was 0.6 m, then $\Pi_{\bar{2}}$=3815.22.

Design of $\Pi_{\bar{3}}$: Because X was fixed, the variable $\Pi_{\bar{3}}$

would vary with d, d was set to 0.045 m and X was 0.6 m, then $\Pi_{\bar{3}}$=0.075.

Design of $\Pi_{\bar{4}}$: Because X was fixed, the variable $\Pi_{\bar{4}}$ would vary with L, L was set to 0.075 m and X was 0.6 m, then $\Pi_{\bar{4}}$=0.125.

To confirm the effectiveness of the combination equation, it was necessary to set one of $\Pi_{\bar{2}}$ $\Pi_{\bar{3}}$ and $\Pi_{\bar{4}}$ to be another fixed value. Here, let the value of L be 0.125 m, then $\Pi_{\bar{4}}$=0.21. The experimental scheme is listed in Table 6.

Table 6 Experimental design of Π equations of $\left(\Pi_{1/5}\right)_{\bar{2},\bar{3},\bar{4}}$ and $\left(\Pi_{1/5}\right)_{\bar{2},\bar{3},\bar{4}}$

No.	ρ/kg·m^{-3}	X/m	μ/Pa·s	Q/m^3·s^{-1}	d/m	L/m	Y_1/m	Y_2/m	Y_3/m
1	1.17	0.6	1.84×10^{-5}	0.036	0.045	0.075(**0.125**)	**0.7000**	**0.5000**	**0.3000**
2	1.17	0.6	1.84×10^{-5}	0.036	0.045	0.075(**0.125**)	**0.7875**	**0.5625**	**0.3375**
3	1.17	0.6	1.84×10^{-5}	0.036	0.045	0.075(**0.125**)	**0.8750**	**0.6250**	**0.3750**
4	1.17	0.6	1.84×10^{-5}	0.036	0.045	0.075(**0.125**)	**0.9625**	**0.6875**	**0.4125**
5	1.17	0.6	1.84×10^{-5}	0.036	0.045	0.075(**0.125**)	**1.0500**	**0.7500**	**0.4500**

4 Results and analysis

4.1 Results of simulation experiment

4.1.1 The total flow rate of the inlet branch pipe

The simulation experiment results of the total flow rate Q of the inlet branch pipe are shown in Figures 6 and 7. From the analysis of Figure 6a and Equation (6), it could be seen that there were significant differences in the P_{out} value of each outlet branch pipe near the U-U boundary. The maximum and minimum values of P_{out} appeared at outlet branch pipe 1 and 4 respectively; while the value of Φ_{1y} shows a decreasing trend with the change of the location of the outlet branch pipe monitoring point, and this trend did not change with the increase of Q. At the I-I boundary, the difference of P_{in} values of each outlet branch pipe was not significant, which means that the difference of Φ_1 values at the I-I boundary was not significant. When Q=0.018 m^3/s, Φ_1 value showed an increasing trend, and when Q≥0.027 m^3/s, Φ_1 value showed a decreasing trend. Comparing the trends of Φ_{1y} and Φ_1, and with the analysis of Equation (7), it could be seen that the difference in the P_{in} value at the I-I boundary was not the main reason for the significant difference in P_{out} value at the U-U boundary and that the difference of H value of each outlet branch pipe was the main reason for the above phenomenon.

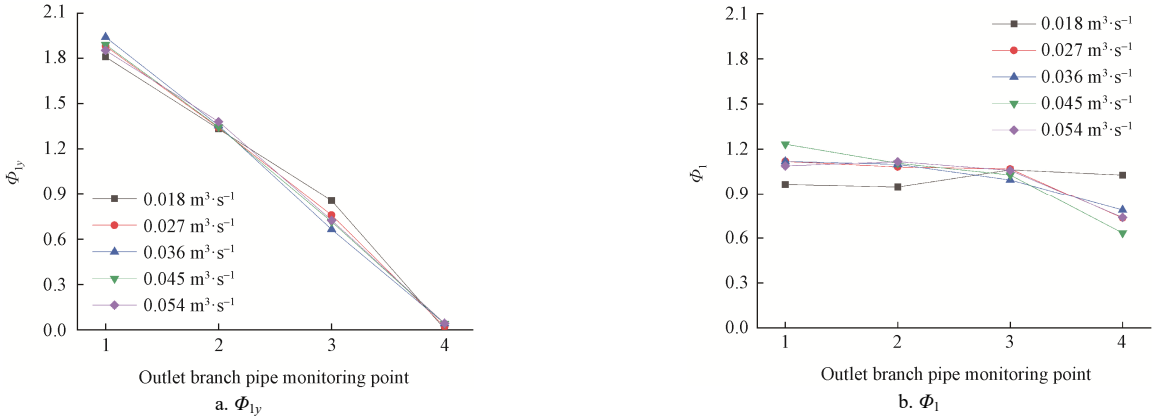

a. Φ_{1y} b. Φ_1

Figure 6 Trends of Φ_{1y} and Φ_1 with the total flow rate of the inlet branch pipes

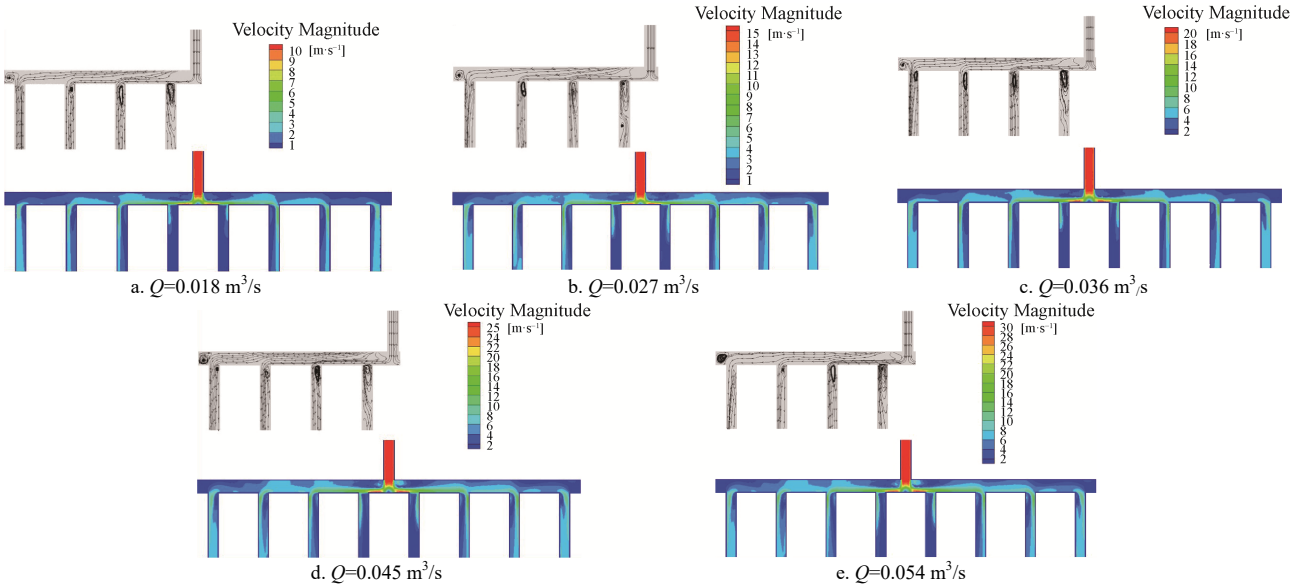

a. Q=0.018 m^3/s b. Q=0.027 m^3/s c. Q=0.036 m^3/s

d. Q=0.045 m^3/s e. Q=0.054 m^3/s

Figure 7 Trends of velocity streamline chart and velocity contour with the total flow rate of the inlet branch pipes

To determine the reason for the difference in the H value of each outlet branch pipe, the flow of air in the pipe was analyzed in conjunction with Figure 7. It can be seen from Figures 7a-7e, the airflow did not turn directly into the header due to the inertia of the

airflow, but finished turning after contacting with the windward side of the wall of the header, and entered both sides of the header, at which the flow velocity on the windward side of the header is obviously higher than that on the leeward side, and under the influence of the velocity difference, the airflow on the leeward side is shifted to the windward side and becomes more and more significant with the increase of Q value. When airflow through the tee, part of the airflow turns to diverge under the action of the ambient pressure difference between the header and the outlet branch pipe, and another part of the unaffected airflow continues to flow along the header axially, after the continuing divergence of the tee position reduces the velocity of the air flow along the header axially, and also reduces the velocity difference between the header windward side and the backwind side. Until near the closed end of the header, the velocity was uniformly distributed, which was consistent with the trend of velocity change reflected by the velocity contour. At this time, combined with Equation (2), it could be seen that the pressure difference in the pipe drives the fluid to continue to flow under the decreasing velocity of the header so that the Φ_1 value of each outlet branch pipe was maintained in a stable range. Therefore, the velocity of the fluid on the windward side of the outlet branch pipe was higher and the velocity on the leeward side was lower, and the velocity difference between the two sides made the *I-I* boundary generate a vortex area, at which time the local loss was the main expression of the H value of each outlet branch pipe. The initial value of the velocity of the air flow into the rest of the outlet branch pipe gradually decreased, the velocity difference between the windward and leeward side of the outlet branch decreased, the area of the vortex area decreased, and the H value of the outlet branch pipe also decreased; therefore, the difference in the H value of the outlet branch pipe was the main reason for the difference in the P_{out} value of the *U-U* boundary.

4.1.2 The inner diameter of the outlet branch pipe

The results of simulation experimental for the inner diameter of the outlet branch pipe d are shown in Figures 8 and 9. From the analysis of Figure 8, It could be seen that when d≤0.03 m, the difference of P_{out} value of each outlet branch pipe at the *U-U* boundary was small; when d≥0.045 m, the P_{out} value of each outlet branch pipe at *U-U* boundary was significant. And the maximum and minimum values of P_{out} appeared at outlet branch pipes 1 and 4, respectively, and the Φ_{2y} value showed a decreasing trend with the change of the location of the outlet branch pipe monitoring point, and did not change with the value of d. When d≤0.03 m, the Φ_{2y} value decreased slightly and the difference was relatively small; when d≥0.045 m, the decreased of the Φ_{2y} value was obvious and difference was significant. It could be seen from Figure 8b and Equation (6) that when d≤0.03 m, the Φ_2 value showed an increasing trend, and the Φ_2 value at the outlet branch pipe monitoring points 1-3 were almost equal; when d≥0.045 m, the Φ_2 value generally showed a decreasing trend, and the differences of Φ_2 values at the monitoring points 1-4 of the outlet branch pipe was not obvious; therefore, the difference of P_{in} values at the *I-I* boundary was relatively small. Comparing the trends of Φ_{2y} and Φ_2, it could be seen that when d≤0.03 m, the H value of the outlet branch pipe did not significantly affect the consistency level of the P_{out} value of each outlet branch pipe except for outlet branch pipe 4; When d≥0.045 m, the influence of the H value of each outlet branch pipe on the P_{out} value of the *U-U* boundary was not ignored; thus, it could be seen that the change of the d value had a significant influence on the consistency of the P_{out} value around the *U-U* boundary.

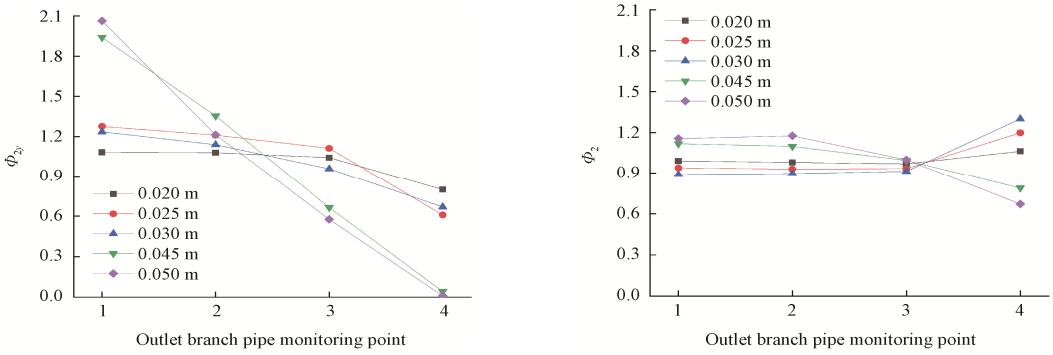

a. Φ_{2y} b. Φ_2

Figure 8 Trends of Φ_{2y} and Φ_2 with the inner diameter of the outlet branch pipes

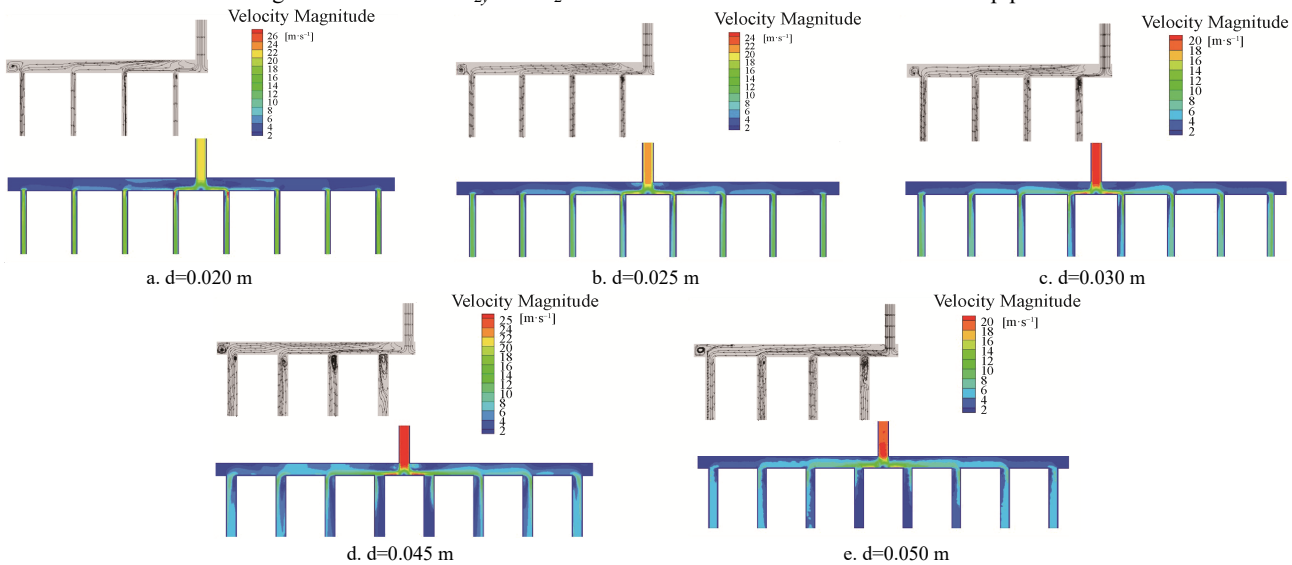

a. d=0.020 m b. d=0.025 m c. d=0.030 m

d. d=0.045 m e. d=0.050 m

Figure 9 Trends of velocity streamline chart and velocity contour with the inner diameter of the outlet branch pipes

To determine the changing trend of the H value of each outlet branch pipe, the flow of airflow in the pipe was analyzed by combining Figure 9. From Figures 9a-9e, It could be seen that the air flows into the header from the inlet branch pipe, under the influence of the velocity difference between the windward sidewall and leeward side of the header, the airflow on the leeward side of the header shifted to the windward side, and with the increase of d value, the shift range increased, and then the air continued to flow along the axial direction of the header, but the air on the windward side of the header was always larger than that on the leeward side, and a wavy velocity distribution appeared at the junction of the outlet branch pipe, and with the increase of d value, the velocity in the diameter direction of the header also showed a certain gradient distribution, and the velocity distribution tends to be stable near the closed end of the header. the main reason for the above phenomenon is that, in the axial direction of the header, due to the influence of the ambient pressure difference, part of the airflow at the tee position of the multi-branch pipe turned into the outlet branch pipe, but due to air inertia, the remaining unaffected airflow continues to move along the header after decelerating and turned at the next tee position, thus forming a wavy velocity contour; as the d value increased, the airflow in the axial direction of the header was more and more influenced by the pressure difference, and the affected air turned to a larger extent. The greater the range of air, the more obvious the wavy velocity distribution in the pipe; along the diameter direction of the header, because the air flow velocity on the leeward side was less than the windward side, the header diameter flow velocity was gradually decreasing, the airflow at different locations in the header diameter was affected by the environmental pressure difference of multiple outlet branch pipes, with the axial airflow movement velocity decreased gradually turn to the outlet branch pipe affecting its flow, so in the header diameter, the airflow velocity was gradually decreasing. the velocity distribution of different gradients was formed in the header diameter, which became more and more obvious with the increase of d value. In each outlet branch pipe, when d≤0.025 m, combined with Figures 9a and 9b, the airflow velocity in the outlet branch pipe was much higher than the header, the velocity was more uniform, and the maximum velocity of the pipe appeared in the outlet branch pipe 4. The main reason was that in the tee position, due to the sudden reduction of the inner diameter of the outlet branch pipe, the air at the junction of the tee did not all change to adapt to the flow trend of the inner diameter of the outlet branch pipe size, at this time, the airflow after turning all and could not flow into the outlet branch pipe, so the airflow in the I-I boundary began to accelerate the airflow, combined with the analysis of Equation (7), before and after entering the outlet branch pipe flow rate and P_{in} value remains unchanged under the assumption that the P_{2y} value at the I-I boundary decreases and the V_{2y} value increased, and because the flow velocity on the windward side of the acceleration into the outlet branch pipe 4 was higher than that on the leeward side, a vortex area was formed on the leeward side of the outlet branch pipe 4, so the H value of the outlet branch pipe 4 was larger than that of other outlet branch pipes, and thus the P_{out} value at the U-U boundary was the smallest. With the continuous diversion of the header and the decrease of the airflow velocity on the windward side, the inertia of the airflow was decreased, and the velocity difference between the windward side and the leeward side of the outlet branch was not enough to form a large vortex area. When d≥0.03 m, combined with Figures 9c-9e, it could be seen that multiple vortex area of unequal area start to appear in the outlet branch pipes 1-4 in turn, and the area of the vortex area increased with the increase of d value; the main reason was: with the increase of d value, the difference between the inner diameter of the outlet branch pipe and the header gradually decreased, and the air after steering had more space to enter the outlet branch pipe, at this time, combined with the analysis of Equation (7), under the assumption that the air velocity and P_{in} value before and after entering the outlet branch pipe remain unchanged, the P_{2y} value at the I-I boundary increased and the V_{2y} value decreased, the flow velocity into the outlet branch pipe decreased, and the air velocity on the windward side of the outlet branch pipe was still higher than that on the leeward side due to the inertia of the turning fluid, so a larger area of the vortex area was formed, and the area of the vortex area becomes larger with the increase of d value, and the local loss was the main form of the H value at generation at this time, which also made a significant difference in the P_{out} value at the U-U boundary.

4.1.3 The length of the closed end of the header

The simulation experiment results of the closed end L of the header pipe are shown in Figures 10 and 11. As shown in Figure 10a and Equation (6), the difference in P_{out} of each outlet branch pipe at the U-U boundary was significant, and the maximum and minimum values of P_{out} appeared at outlet branch pipes 1 and 4, respectively, value decreased with the change of the location of the outlet branch pipe monitoring point, and the decreasing curve did not differ significantly with the change of L value. As shown in Figure 10b and Equation (6), the difference of P_{in} and Φ_3 values at the I-I boundary for each outlet branch pipe was not significant, and the decreasing curve of Φ_3 value did not show significant difference with the increase of L value. Comparing the trends of Φ_{y3} and Φ_3 values, it could be seen that the difference in H values of each outlet branch pipe made significant difference in P_{out} value at the U-U boundary.

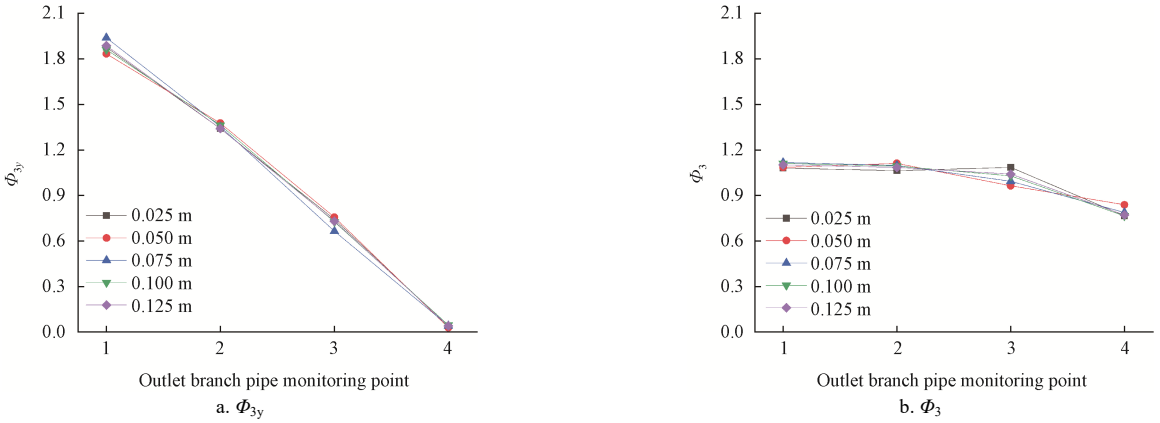

Figure 10 Trends of Φ_{3y} and Φ_3 variation with the length of the closed end of the header

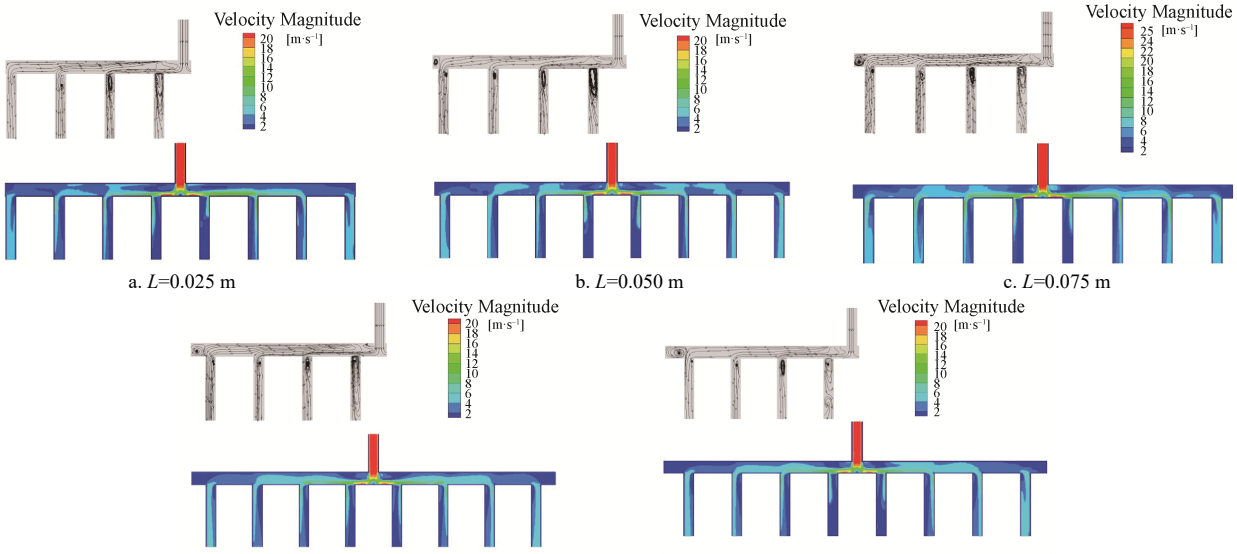

Figure 11 Trend of velocity streamline chart and velocity contour with the length of the closed end of the header

To determine the reasons for the difference in H values of each outlet branch pipe, the flow of air in the pipe was analyzed in combination with Figure 12. From Figures 11a-11e, it could be seen that when L≤0.05 m, the airflow on the windward side of the header axially showed a discontinuous wave-like distribution, and a discontinuous area of low velocity and high velocity is formed with the outlet branch pipe position as the boundary, while the velocity contour on the leeward side of the header also shows a similar distribution state; in the header diameter to the center line of the header as the boundary, also formed a low velocity and high velocity area of the hierarchical contour distribution, until the closed end of the header, the air velocity distribution is still uneven. When L=0.05 m, a certain area of vortex area began to appear at the end of the header. When L≥0.075 m, the air velocity gradually decreased along the axial direction of the header, showing a continuous wavy velocity distribution, with the increase of L value, the axial velocity of the header with the outlet branch pipe position as the boundary showed an obvious downward trend, and the velocity distribution became more uniform; meanwhile, between the windward and leeward side of the header diameter, the velocity also showed a stable distribution from high to low, and the gradient distribution became more uniform with the increase of L value. From Figures 11a-11e, it could be seen that the outlet branch pipes 1-4 all form a vortex area with a certain area, the vortex area of the outlet branch pipe 4 increases with the increase of L value; the vortex area of the outlet branch pipe 3 had no obvious change with the increase of L value; and the vortex area of the outlet branch pipes 1 and 2 increases with L value, the overall increase showed a trend of first increasing and then decreasing. The main reason for the above phenomenon was that: When L=0.025 m, under the influence of the gradual decrease of the air velocity of the header and the gradual increase of the pressure, the P_{in} value of each outlet branch pipe around the I-I boundary was relatively stable; however, at the closed end of the header, part of the undirected airflow entering the outlet branch pipe 1 collides with the pipe wall, resulting in a certain local loss, so that the flow velocity in the outlet branch pipe 1 was lower than the other level, the velocity difference between the windward side and the leeward side was small, so no obvious vortex area was formed; and the loss along the way was the main expression of the H value in outlet branch pipe 1, because there was a large vortex area in outlet branch pipes 2-4, the local loss was the main manifestation of the H value in outlet branch pipe 2-4, which in turn results in a large difference in the P_{out} value of each outlet branch pipe at the U-U boundary. When 0.050≤L≤0.75 m, the airflow formed a certain vortex area at the end of the closed end of the header, and the airflow from the vortex area entered the outlet branch pipe 1 with the header turning air under the action of pressure difference, at this time, the air velocity on the windward side was greater than that on the leeward side, and the larger velocity difference formed a vortex area there, and the area of the vortex area increased with the increase of L value, at this time, the local loss was the main manifestation of the H value of outlet branch pipe; the difference area of the vortex area made the P_{out} value of each outlet branch pipe at the U-U boundary appeared more difference. When L≥0.1 m, the airflow in the vortex area at the end of the header pipe moves slowly and the airflow into the outlet branch pipe 1 decreased, at this time the air on the windward side of the outlet branch pipe 1 was mainly steering flow, with the increase L value, the velocity difference between the windward side and the leeward side of the airflow decreased and the area of the formed vortex area decreased. Meanwhile, there are still vortex areas with different areas in the other outlet branch pipes, so the local loss was the main manifestation of the H value of each outlet branch pipe, at this time, which also causes the P_{out} value of each outlet branch pipe at the U-U boundary to be quite different.

4.1.4 The outlet branch pipe spacing

The results of the simulation experiment for the outlet branch pipe spacing δ are shown in Figures 12 and 13. From Figure 12a and Equation (6), it could be seen that the P_{out} values for each outlet branch pipe at the U-U boundary differ significantly, and the maximum and minimum values of P_{out} values appeared at the outlet branch pipes 1 and 4, respectively; and the Φ_{4y} values showed a decreasing trend with the change of the location of the outlet branch pipe monitoring point, and the trend did not show a significant difference with the change of δ value. From Figure 12b and Equation (6), the P_{in} difference of each outlet branch pipe around the I-I boundary is not significant, when δ≤0.25 m, the Φ_4 value showed a decreasing trend at the I-I boundary, when δ=0.275 m, the Φ_4 value was nearly a straight line at the I-I boundary, and when δ=0.3 m, the Φ_4 values showed an increasing trend at the I-I boundary. Comparing the trends of Φ_{4y} and Φ_4 with the analysis of Equation (7), it could be seen that the different H values of each outlet branch pipe made significant differences in P_{out} values at the U-U boundary.

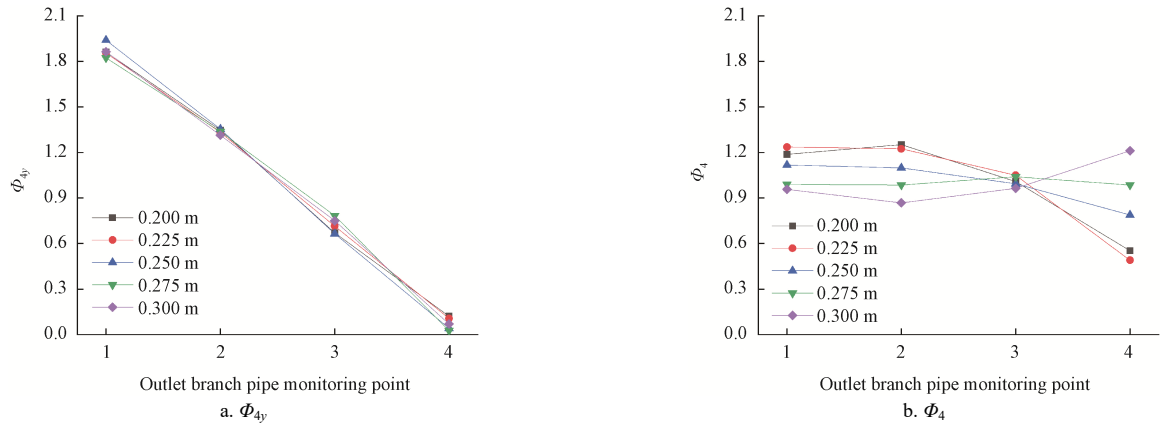

a. Φ_{4y} b. Φ_4

Figure 12 Trend of Φ_{4y} and Φ_4 variation with the outlet branch pipe spacing

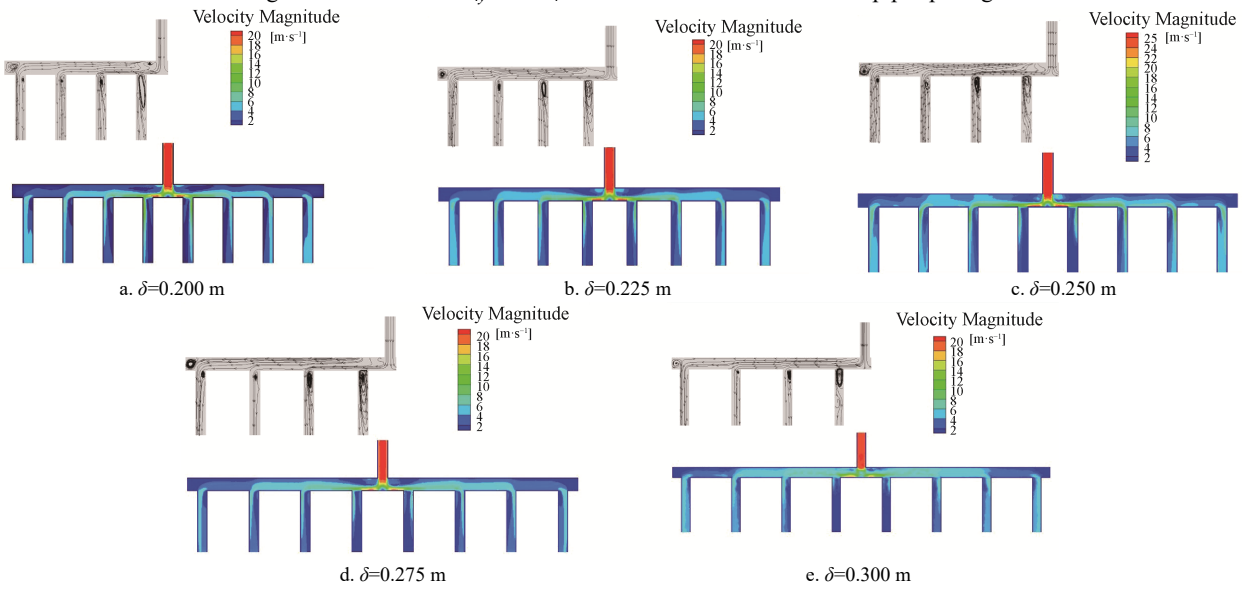

a. δ=0.200 m b. δ=0.225 m c. δ=0.250 m

d. δ=0.275 m e. δ=0.300 m

Figure 13 Trends of velocity streamline chart and velocity contour with the outlet branch pipe spacing

To investigate the trend of the H value of each outlet branch pipe, the flow of air was analyzed in combination with Figure 13, From Figures 13a-13e, it could be seen that with the value of δ increases, the velocity distribution in the header was gradually uniform, when $\delta \leq 0.275$ m, the airflow velocity in the axial direction of the header was continuous wave-shaped distribution characteristics, due to the inertia of the airflow, the airflow on the windward side of the header was significantly larger than that on the leeward side, the airflow velocity difference between the leeward side and the windward side was shifted. When δ=0.2 m, even a certain area of vortex area was formed, which caused local loss, and the range of airflow offset decreased with the increase of δ. In the radial of the header, different velocity gradients are formed between the windward and leeward sides of the header, but with the increase of δ, the velocity difference between the leeward and windward sides of the header decreased, and the velocity gradient was not obvious; to the end of the header, the velocity values were nearly uniformly distributed. When δ=0.3 m, the velocity difference between the windward and leeward sides of the header decreased, and the velocity distribution in the header was uniform. From Figures 13a-13e, it could be seen that the vortex area formed in the outlet branch pipe 1-4, and the area of vortex area showed a decreasing trend with the increase of δ value. The reason for the above phenomenon was: the larger the value of δ, the airflow from the inlet branch pipe into the header to recover to a stable flow state, reducing the local loss of airflow in the header, the overall decrease in the airflow velocity in the header, the velocity distribution no longer appeared more obvious boundary layer; therefore, when $\delta \leq 0.25$ m, the P_{in} value of outlet branch pipe 4 was lower than the other outlet branch pipes, and when $\delta \geq 0.275$ m, the P_{in} value of outlet branch pipe 4 was higher than the other outlet branch pipes, the increase of the δ value made the airflow section in the header longer, the velocity difference between the windward and leeward side of each outlet branch pipe was reduced, and the area of the vortex area formed was also reduced, but at this time the local loss was still the main expression of the H value in each outlet branch pipe, and was also the main reason for the difference in the P_{out} value of each outlet branch pipe at the U-U boundary.

In summary, due to the complex situation of airflow movement in the multi-branch pipe, it is difficult to estimate the vortex area in the outlet branch pipe through a fixed quantitative index, and if the generalization is done through the conventional experimental design, it requires a lot of experimental cost and effort and increases the research period. The dimensional analysis method, as a research method that can relatively quickly establish the functional relationship between the multi experiment factors and the solution indicators, can summarize the empirical laws in the experimental results, and establish the parameterized prediction equations of the experiment factors and experiment indicators. The optimal design of the multi-branch pipe structure provides the necessary basic support, so it is necessary to establish a universally applicable multi-branch pipe outlet parameter index prediction equation.

4.2 The bench test results

In order to investigate the influence of the geometric mechanism and working parameters of the multi-branch pipe on the air parameters of the inlet and outlet branch pipes from a macroscopic point of view,

an experiment was conducted at the Key Laboratory of Key Technology on Agricultural Machine and Equipment (South China Agricultural University), where the outlet branch pipes were numbered 1-8 in the order from left to right, according to the experimental design scheme in Tables 3-6. Record the airflow parameters of each group of outlet branch pipes, repeat three times for each outlet branch pipe, select the average value of the test results, record the experimental data in Tables 7-10, and use CurveFitter software to perform polynomial fitting on the corresponding experimental data in Tables 7-10 combined processing.

Table 7 Results and Π equations of $\left(\Pi_{1/2}\right)_{\bar{3},\bar{4},\bar{5}}$ and $\left(\Pi_{1/2}\right)_{\bar{3},\bar{4},\bar{\bar{5}}}$

Q/m^3·s^{-1} (Outlet branch pipe 1)	d=0.045 m, L=0.075 m, Y_1=0.875 m $\bar{\Pi}_3=0.075$, $\bar{\Pi}_4=0.125$, $\bar{\Pi}_5=1.46$			d=0.045 m, L=0.075 m, Y_1=1.05 m $\bar{\Pi}_3=0.075$, $\bar{\Pi}_4=0.125$, $\bar{\bar{\Pi}}_5=1.75$		
	Π_2	v_1 /m·s^{-1}	Π_1	Π_2	v_1 /m·s^{-1}	Π_1
0.018	1907.61	2.26	86223.91	1907.61	2.04	77830.43
0.027	2861.41	3.64	138873.91	2861.41	3.09	117890.22
0.036	3815.22	5.04	**192286.96**	3815.22	4.18	159476.00
0.045	4967.02	6.22	237306.52	4967.02	5.38	205258.70
0.054	5722.83	7.35	280418.48	5722.83	6.64	253330.43
	$\Pi_1=2.32\times10^{-9}\Pi_2^4-3.42\times10^{-5}\Pi_2^3+0.18\Pi_2^2-333.30\,\Pi_2-280927$ $R^2=1$			$\Pi_1=1.54\times10^{-9}\Pi_2^4-2.18\times10^{-6}\Pi_2^3+0.11\Pi_2^2-195.82\Pi_2-179892$ $R^2=1$		
Q/m^3·s^{-1} (Outlet branch pipe 2)	d=0.045 m, L=0.075 m, Y_2=0.625 m $\bar{\Pi}_3=0.075$, $\bar{\Pi}_4=0.125$, $\bar{\Pi}_5=1.04$			d=0.045 m, L=0.075 m, Y_2=0.75 m $\bar{\Pi}_3=0.075$, $\bar{\Pi}_4=0.125$, $\bar{\bar{\Pi}}_5=1.25$		
	Π_2	v_2 /m·s^{-1}	Π_1	Π_2	v_2 /m·s^{-1}	Π_1
0.018	1907.61	1.94	74015.22	1907.61	1.76	67147.83
0.027	2861.41	3.07	117127.17	2861.41	2.63	100340.22
0.036	3815.22	4.21	**160620.64**	3815.22	3.52	134295.65
0.045	4967.02	5.25	200298.91	4967.02	4.53	172829.35
0.054	5722.83	6.34	241884.78	5722.83	5.59	213270.65
	$\Pi_1=1.94\times10^{-9}\Pi_2^4-2.82\times10^{-5}\Pi_2^3+0.14\Pi_2^2-267.32\,\Pi_2+227556$ $R^2=1$			$\Pi_1=1.18\times10^{-9}\Pi_4^4-1.65\times10^{-5}\Pi_4^3+0.083\Pi_4^2-141.43\,\Pi_4+134827$ $R^2=1$		
Q/m^3·s^{-1} (Outlet branch pipe 3)	d=0.045 m, L=0.075 m, Y_3=0.375 m $\bar{\Pi}_3=0.075$, $\bar{\Pi}_4=0.125$, $\bar{\Pi}_5=0.63$			d=0.045 m, L=0.075 m, Y_3=0.45 m $\bar{\Pi}_3=0.075$, $\bar{\Pi}_4=0.125$, $\bar{\bar{\Pi}}_5=0.75$		
	Π_2	v_3 /m·s^{-1}	Π_1	Π_2	v_3 /m·s^{-1}	Π_1
0.018	1907.61	1.56	58917.39	1907.61	1.44	54939.13
0.027	2861.41	2.31	88245.98	2861.41	2.36	90039.13
0.036	3815.22	2.95	**112548.91**	3815.22	2.80	106826.09
0.045	4967.02	3.83	146122.83	4967.02	3.47	132388.04
0.054	5722.83	4.60	175500.00	5722.83	4.21	160620.45
	$\Pi_1=-7.89\times10^{-11}\Pi_2^4+2.54\times10^{-6}\Pi_2^3-0.026\Pi_2^2+89.66\,\Pi_2-53639.5$ $R^2=1$			$\Pi_1=-5.21\times10^{-10}\Pi_3^4+1.11\times10^{-5}\Pi_3^3-0.079\Pi_3^2+251.54\,\Pi_3-207454$ $R^2=1$		

Note: The bolded data indicate the value of each outlet branch pipe in Equation (10). The same as Tables 8, 9, and 10.

Table 8 Results and Π equations of $\left(\Pi_{1/3}\right)_{\bar{2},\bar{4},\bar{5}}$ and $\left(\Pi_{1/3}\right)_{\bar{2},\bar{4},\bar{\bar{5}}}$

d/ m (Outlet branch pipe 1)	Q=0.036 m^3·s^{-1}, L=0.075 m, Y_1=0.875 m $\bar{\Pi}_2=3815.22$, $\bar{\Pi}_4=0.125$, $\bar{\Pi}_5=1.46$			Q=0.036 m^3·s^{-1}, L=0.075 m, Y_1=1.05 m $\bar{\Pi}_2=3815.22$, $\bar{\Pi}_4=0.125$, $\bar{\bar{\Pi}}_5=1.75$		
	Π_3	v_1/m·s^{-1}	Π_1	Π_3	v_1/m·s^{-1}	Π_1
0.020	0.033	15.27	582583.70	0.033	15.51	591740.22
0.025	0.043	10.28	392433.26	0.043	10.29	392585.87
0.030	0.050	7.62	290719.57	0.050	7.42	283089.13
0.045	0.075	5.04	**192286.96**	0.075	4.18	159476.09
0.050	0.083	4.46	170158.70	0.083	4.14	159750.00
	$\Pi_1=-1.80\times10^{11}\Pi_2^4+3.77\times10^{10}\Pi_2^3-2.58\times10^{9}\Pi_3^2+5.24\times10^{7}\Pi_3+514089$ $R^2=1$			$\Pi_1=-1.32\times10^{11}\Pi_2^4+2.80\times10^{10}\Pi_2^3-1.92\times10^{9}\Pi_3^2+3.19\times10^{7}\Pi_3+767238$ $R^2=1$		
d/ m (Outlet branch pipe 2)	Q=0.036 m^3·s^{-1}, L=0.075 m, Y_2=0.625 m $\bar{\Pi}_2=3815.22$, $\bar{\Pi}_4=0.125$, $\bar{\Pi}_5=1.04$			Q=0.036 m^3·s^{-1}, L=0.075 m, Y_2=0.75 m $\bar{\Pi}_2=3815.22$, $\bar{\Pi}_4=0.125$, $\bar{\bar{\Pi}}_5=1.25$		
	Π_3	v_2/m·s^{-1}	Π_1	Π_3	v_2/m·s^{-1}	Π_1
0.020	0.033	15.24	581439.13	0.033	15.28	582965.22
0.025	0.043	10.01	381903.26	0.043	10.10	385336.96
0.030	0.050	7.32	279273.91	0.050	7.11	271261.96
0.045	0.075	4.21	**160620.65**	0.075	3.52	134295.65
0.050	0.083	3.42	130480.43	0.083	3.32	126665.22
	$\Pi_1=-1.39\times10^{11}\Pi_3^4+2.80\times10^{10}\Pi_3^3-1.73\times10^{9}\Pi_3^2+2.66\times10^{7}\Pi_3+942320$ $R^2=1$			$\Pi_1=-1.64\times10^{11}\Pi_3^4+3.62\times10^{10}\Pi_3^3-2.61\times10^{9}\Pi_3^2+5.74\times10^{7}\Pi_3+423314$ $R^2=1$		
d/ m (Outlet branch pipe 3)	Q=0.036 m^3·s^{-1}, L=0.075 m, Y_3=0.375 m $\bar{\Pi}_2=3815.22$, $\bar{\Pi}_4=0.125$, $\bar{\Pi}_5=0.63$			Q=0.036 m^3·s^{-1}, L=0.075 m, Y_2=0.45 m $\bar{\Pi}_2=3815.22$, $\bar{\Pi}_4=0.125$, $\bar{\bar{\Pi}}_5=0.75$		
	Π_3	v_3/m·s^{-1}	Π_1	Π_3	v_3/m·s^{-1}	Π_1
0.020	0.033	14.98	571519.57	0.033	15.05	574190.22
0.025	0.043	9.59	365879.35	0.043	9.72	370839.13
0.030	0.050	6.71	256001.09	0.050	6.61	252185.87
0.045	0.075	2.95	**112548.91**	0.075	2.80	106826.09
0.050	0.083	2.36	90039.31	0.083	2.15	82027.17
	$\Pi_1=-1.23\times10^{11}\Pi_3^4+2.53\times10^{10}\Pi_3^3-1.60\times10^{9}\Pi_3^2+1.77\times10^{7}\Pi_3+958948$ $R^2=1$			$\Pi_1=-2.03\times10^{11}\Pi_3^4+4.45\times10^{10}\Pi_3^3-3.24\times10^{9}\Pi_3^2+7.73\times10^{7}\Pi_3+191861$ $R^2=1$		

Table 9 Results and Π equations of $\left(\Pi_{1/4}\right)_{\bar{2},\bar{3},\bar{5}}$ and $\left(\Pi_{1/4}\right)_{\bar{2},\bar{3},\bar{\bar{5}}}$

L/ m (Outlet branch pipe 1)	Q=0.036 m$^3\cdot$s^{-1}, d=0.045 m, Y_1=0.875 m $\bar{\Pi}_2$ = 3815.22, $\bar{\Pi}_3$ = 0.075, $\bar{\Pi}_5$ = 1.46			Q=0.036 m$^3\cdot$s^{-1}, d=0.045 m, Y_1=1.05 m $\bar{\Pi}_2$ = 3815.22, $\bar{\Pi}_3$ = 0.075, $\bar{\bar{\Pi}}_5$ = 1.75		
	Π_4	v_1/ m$\cdot$s^{-1}	Π_1	Π_4	v_1/ m$\cdot$s^{-1}	Π_1
0.025	0.042	4.91	187327.17	0.042	4.65	177407.61
0.050	0.083	4.78	182367.39	0.083	4.79	182748.91
0.075	0.125	5.04	**192286.96**	0.125	4.18	159476.09
0.010	0.170	4.93	188090.42	0.170	4.61	175881.52
0.125	0.210	4.90	186945.65	0.210	4.39	167488.04
	Π_1=5.89×10$^8\Pi_4^4$–3.11×10$^8\Pi_4^3$+5.64×10$^7\Pi_4^2$–4.04×10$^6\Pi_4$+278602 R^2=1			Π_1=–1.69×10$^9\Pi_4^4$+8.55×10$^8\Pi_4^3$–1.49×10$^8\Pi_4^2$+1.02×10$^7\Pi_4$–45732 R^2=1		
L/ m (Outlet branch pipe 2)	Q=0.036 m$^3\cdot$s^{-1}, d=0.045 m, Y_2=0.625 m $\bar{\Pi}_2$ = 3815.22, $\bar{\Pi}_3$ = 0.075, $\bar{\Pi}_5$ = 1.04			Q=0.036 m$^3\cdot$s^{-1}, d=0.045 m, Y_2=0.75 m $\bar{\Pi}_2$ = 3815.22, $\bar{\Pi}_3$ = 0.075, $\bar{\bar{\Pi}}_5$ = 1.25		
	Π_4	v_2/ m$\cdot$s^{-1}	Π_1	Π_4	v_2/m$\cdot$s^{-1}	Π_1
0.025	0.042	4.15	158331.52	0.042	3.87	136203.26
0.050	0.083	4.14	157950.00	0.083	4.00	152608.70
0.075	0.125	4.21	**160620.65**	0.125	3.52	134295.65
0.010	0.170	4.22	161002.17	0.170	3.85	146885.87
0.125	0.210	4.13	157568.48	0.210	3.70	141163.04
	Π_1=4.80×10$^7\Pi_4^4$–3.20×10$^7\Pi_4^3$+6.79×10$^6\Pi_4^2$–521555Π_4+ 170484 R^2=1			Π_1=–1.47×10$^9\Pi_4^4$+7.60×10$^8\Pi_4^3$–1.36×10$^8\Pi_4^2$+9.81×10$^6\Pi_4$–86910.7 R^2=1		
L/ m (Outlet branch pipe 3)	Q=0.036 m$^3\cdot$s^{-1}, d=0.045 m, Y_3=0.375 m $\bar{\Pi}_2$ = 3815.22, $\bar{\Pi}_3$ = 0.075, $\bar{\Pi}_5$ = 0.63			Q=0.036 m$^3\cdot$s^{-1}, d=0.045 m, Y_3=0.45 m $\bar{\Pi}_2$ = 3815.22, $\bar{\Pi}_3$ = 0.075, $\bar{\bar{\Pi}}_5$ = 0.75		
	Π_4	v_3 /m$\cdot$s^{-1}	Π_1	Π_4	v_3 /m$\cdot$s^{-1}	Π_1
0.025	0.042	3.09	117890.22	0.042	2.96	112930.43
0.050	0.083	3.07	117127.17	0.083	3.01	114838.04
0.075	0.125	2.95	**112548.91**	0.125	2.80	106826.09
0.010	0.170	3.08	117508.70	0.170	2.89	110259.78
0.125	0.210	3.05	116364.13	0.210	2.90	110641.30
	Π_1=–3.62×10$^8\Pi_4^4$+1.80×10$^8\Pi_4^3$–3.05×10$^7\Pi_4^2$+1.99×10$^6\Pi_4$+ 75738 R^2=1			Π_1=–4.56×10$^8\Pi_4^4$+2.38×10$^8\Pi_4^3$–4.26×10$^7\Pi_4^2$+2.97×10$^6\Pi_4$ + 47019.5 R^2=1		

Table 10 Results and Π equations of $\left(\Pi_{1/5}\right)_{\bar{2},\bar{3},\bar{4}}$ and $\left(\Pi_{1/5}\right)_{\bar{2},\bar{3},\bar{\bar{4}}}$

Y_1/ m	Q=0.036 m$^3\cdot$s^{-1}, d=0.045 m, L=0.075 m $\bar{\Pi}_2$ = 3815.22, $\bar{\Pi}_3$ = 0.075, $\bar{\Pi}_4$ = 0.125			Q=0.036 m$^3\cdot$s^{-1}, d=0.045 m, L=0.125 m $\bar{\Pi}_2$ = 3815.22, $\bar{\Pi}_3$ = 0.075, $\bar{\bar{\Pi}}_4$ = 0.21		
	Π_5	v_1/m$\cdot$s^{-1}	Π_1	Π_5	v_1/m$\cdot$s^{-1}	Π_1
0.7000	1.17	5.22	199154.35	1.17	5.25	200298.91
0.7875	1.31	5.15	196483.70	1.31	5.18	197628.26
0.8750	1.46	5.04	**192286.96**	1.46	4.18	159476.09
0.9625	1.60	4.31	164435.87	1.60	4.70	179315.22
1.0500	1.75	4.30	164054.53	1.75	4.24	161765.22
	Π_1=7.02×10$^7\Pi_4^4$–4.12×10$^7\Pi_5^3$+8.76×10$^7\Pi_5$–8.22×10$^7\Pi_5$+ 2.88767×10^7 R^2=1			Π_1=–1.76×10$^7\Pi_4^4$+1.02×108Π_5^3–2.22×10$^8\Pi_5^2$+2.12×10$^8\Pi_5$–7.53×10^7 R^2=1		
Y_2/ m	Q=0.036 m$^3\cdot$s^{-1}, d=0.045 m, L=0.075 m $\bar{\Pi}_2$ = 3815.22, $\bar{\Pi}_3$ = 0.075, $\bar{\Pi}_4$ = 0.125			Q=0.036 m$^3\cdot$s^{-1}, d=0.045 m, L=0.125 m $\bar{\Pi}_2$ = 3815.22, $\bar{\Pi}_3$ = 0.075, $\bar{\bar{\Pi}}_4$ = 0.21		
	Π_5	v_2/m$\cdot$s^{-1}	Π_1	Π_5	v_2/m$\cdot$s^{-1}	Π_1
0.5000	0.83	4.44	169395.65	0.83	4.47	170540.22
0.5625	0.94	4.34	165580.43	0.94	4.34	165580.43
0.6250	1.04	4.21	**160620.65**	1.04	3.52	134295.65
0.6875	1.15	3.66	139636.96	1.15	4.01	152990.22
0.7500	1.25	3.61	137729.35	1.25	3.76	143452.17
	Π_1=1.59×10$^7\Pi_5^4$–6.49×10$^7\Pi_5^3$+9.84×10$^7\Pi_5^2$–6.57×10$^7\Pi_5$+1.65×10^7 R^2=1			Π_1=–5.40×10$^7\Pi_5^4$+2.25×10$^8\Pi_5^3$–3.48×10$^8\Pi_5^2$+2.38×10$^8\Pi_5$–6.02×10^7 R^2=1		
Y_3/ m	Q=0.036 m$^3\cdot$s^{-1}, d=0.045 m, L=0.075 m $\bar{\Pi}_2$ = 3815.22, $\bar{\Pi}_3$ = 0.075, $\bar{\Pi}_4$ = 0.125			Q=0.036 m$^3\cdot$s^{-1}, d=0.045 m, L=0.125 m $\bar{\Pi}_2$ = 3815.22, $\bar{\Pi}_3$ = 0.075, $\bar{\bar{\Pi}}_4$ = 0.21		
	Π_5	v_3/m$\cdot$s^{-1}	Π_1	Π_5	v_3/m$\cdot$s^{-1}	Π_1
0.3000	0.50	3.13	119416.30	0.50	3.07	117127.07
0.3375	0.56	3.19	121705.43	0.56	2.96	112930.43
0.3750	0.63	2.95	**112548.91**	0.63	2.80	106826.09
0.4125	0.69	2.80	106826.09	0.69	3.07	117127.07
0.4500	0.75	2.73	104155.43	0.75	2.89	110259.78
	Π_1=–2.99×10$^7\Pi_5^4$+7.95×10$^7\Pi_5^3$–7.82×10$^7\Pi_5^2$+3.41×10$^7\Pi_5$–5.36×10^6 R^2=1			Π_1=–1.37×10$^7\Pi_5^4$+3.37×10$^8\Pi_5^3$–3.08×10$^8\Pi_5^2$+1.24×10$^7\Pi_5$ –1.85×10^7 R^2=1		

4.2.1 Fitting of Π equations

The results of each component of the experiments verifying the validity of the Π equation and the fitting curve equation of each component are listed in Tables 7-10. The Π equation is composed of the product of the equations of each component, and its specific expansion form is:

$$\Pi_1 = \frac{f_1\left(\Pi_2\overline{\Pi_3}\overline{\Pi_4}\overline{\Pi_5}\right) f_2\left(\overline{\Pi_2}\Pi_3\overline{\Pi_4}\overline{\Pi_5}\right) f_3\left(\overline{\Pi_2}\overline{\Pi_3}\Pi_4\overline{\Pi_5}\right) f_4\left(\overline{\Pi_2}\overline{\Pi_3}\overline{\Pi_4}\Pi_5\right)}{f\left(\overline{\Pi_2}\overline{\Pi_3}\overline{\Pi_4}\overline{\Pi_5}\right)^{5-2}} \tag{9}$$

where,

$f_1\left(\Pi_2\overline{\Pi_3}\overline{\Pi_4}\overline{\Pi_5}\right), f_2\left(\overline{\Pi_2}\Pi_3\overline{\Pi_4}\overline{\Pi_5}\right), f_3\left(\overline{\Pi_2}\overline{\Pi_3}\Pi_4\overline{\Pi_5}\right), f_4\left(\overline{\Pi_2}\overline{\Pi_3}\overline{\Pi_4}\Pi_5\right)$ represent the component equations fitted by Π_1, Π_2, Π_3 and Π_4, respectively.

It can be seen from the similarity criterion theory[24,26]:

$$\begin{aligned} f\left(\overline{\Pi_2}\overline{\Pi_3}\overline{\Pi_4}\overline{\Pi_5}\right) &= f_1\left(\overline{\Pi_2}\overline{\Pi_3}\overline{\Pi_4}\overline{\Pi_5}\right) = f_2\left(\overline{\Pi_2}\overline{\Pi_3}\overline{\Pi_4}\overline{\Pi_5}\right) \\ &= f_3\left(\overline{\Pi_2}\overline{\Pi_3}\overline{\Pi_4}\overline{\Pi_5}\right) = f_4\left(\overline{\Pi_2}\overline{\Pi_3}\overline{\Pi_4}\overline{\Pi_5}\right) \end{aligned} \tag{10}$$

Combining Equations (9) and (10), the velocity v_1 of outlet branch pipe 1 is obtained from the data in Tables 7-10 as:

$$\begin{aligned} v_1 = &(2.32\times10^{-9}\ (\rho Q/dX)^4 - 3.42\times10^{-5}\ (\rho Q/dX)^3 + 0.18\ (\rho Q/dX)^2 \\ &-333.30\ \rho Q/dX - 280927) \times (-935024.40\ (d/X)^4 - 196266.04 \\ &(d/X)^3 + 13393.11\ (d/X)^2 - 272.63\ d/X + 2.67) \times (3064.74\ (L/X)^4 \\ &-1615.81(L/X)^3 + 293.37\ (L/X)^2 - 21\ L/X + 1.45) \times (37.47\ (Y/X)^4 \\ &-214.32(Y/X)^3 + 455.74\ (Y/X)^2 - 427.31\ (Y/X) + 150.18) \times \mu/\rho X \end{aligned} \tag{11}$$

4.2.2 Verification of Π equations

The combined Π equation and v_1 equation need to be tested three times. The verification method is as follows[25, 27]: 1) The v_1 value and the Π_1 value calculated by the Π equation were compared with the experimental data of each experiment point to verify the validity of the Π equation. 2) The v_1 value and the Π_1 value calculated by the Π equation were compared with the experimental data of the working conditions on both sides of the fitting curve of each component equation to verify the validity of the Π equation. 3) Other test conditions within the application range of the empirical formula are considered to verify the Π validity of the equation.

1) The results of the first validation analysis. The parameters of each experiment point are converted into corresponding Π values and are brought into Equation (11) respectively to obtain the corresponding Π_1 values and v_1 values, and then the data obtained from the Π equation is compared with the experimental data, as listed in Table 11. It can be seen from the table that the deviation between the data calculated by the Π equation and the experimental data is within the acceptable engineering range, that is, the relative deviation of the calculated results at the experimental point is much less than 10%[22], so Equation (11) is relatively accurate.

Table 11 Test of fitting of Π equations and every experiment points

$\overline{\Pi}_3 = 0.075, \overline{\Pi}_4 = 0.125$									
	$\overline{\Pi}_5 = 1.46$			$\overline{\Pi}_5 = 1.04$			$\overline{\Pi}_5 = 0.63$		
Π_2	Π_1^*	v_1^*/m·s^{-1}	Er./%	Π_1^*	v_2^*/m·s^{-1}	Er./%	Π_1^*	v_3^*/m·s^{-1}	Er./%
1907.61	86149.43	2.258	0.086	73791.17	1.934	0.31	58938.82	1.545	0.96
2861.41	138749.30	3.637	0.090	116773.14	3.061	0.29	88278.18	2.313	0.13
3815.22	192108.32	5.035	0.093	160134.40	4.200	0.24	112590.18	2.951	0.03
4967.02	237073.92	6.214	0.098	199694.47	5.234	0.30	146176.75	3.831	0.03
5722.83	280137.77	7.343	0.100	245219.49	6.427	1.37	177788.81	4.660	1.30
$\overline{\Pi}_2 = 3815.22, \overline{\Pi}_4 = 0.125$									
	$\overline{\Pi}_5 = 1.46$			$\overline{\Pi}_5 = 1.04$			$\overline{\Pi}_5 = 0.63$		
Π_3	Π_1^*	v_1^*/m·s^{-1}	Er./%	Π_1^*	v_1^*/m·s^{-1}	Er./%	Π_1^*	v_1^*/m·s^{-1}	Er./%
0.033	582097.81	15.257	0.086	579678.49	15.194	0.30	571552.29	14.981	0.007
0.043	386339.07	10.126	1.550	380746.74	9.980	0.30	365906.83	9.591	0.010
0.050	290471.37	7.613	0.085	278428.87	7.300	0.27	256028.08	6.711	0.015
0.075	192108.32	5.035	0.093	160134.40	4.200	0.24	112590.18	2.951	0.034
0.083	169992.93	4.456	0.097	130089.98	3.410	0.29	90089.48	2.361	0.042
$\overline{\Pi}_2 = 3815.22, \overline{\Pi}_4 = 0.075$									
	$\overline{\Pi}_5 = 1.46$			$\overline{\Pi}_5 = 1.04$			$\overline{\Pi}_5 = 0.63$		
Π_4	Π_1^*	v_1^*/m·s^{-1}	Er./%	Π_1^*	v_2^*/m·s^{-1}	Er./%	Π_1^*	v_3^*/m·s^{-1}	Er./%
0.042	187124.42	4.905	0.110	158261.76	4.148	0.05	117933.71	3.091	0.032
0.083	182184.13	4.775	0.100	157726.95	4.357	5.24	117170.35	3.071	0.033
0.125	192108.32	5.035	0.093	160134.40	4.200	0.24	112590.18	2.951	0.034
0.170	188947.52	4.926	0.076	160118.33	4.197	0.55	117554.28	3.081	0.032
0.210	186850.31	4.898	0.051	156228.52	4.095	0.85	116410.36	3.051	0.033
$\overline{\Pi}_2 = 3815.22, \overline{\Pi}_3 = 0.075, \overline{\Pi}_4 = 0.125$									
	$\overline{\Pi}_5 = 1.46$			$\overline{\Pi}_5 = 1.04$			$\overline{\Pi}_5 = 0.63$		
Π_5	Π_1^*	v_1^*/m·s^{-1}	Er./%	Π_1^*	v_2^*/m·s^{-1}	Er./%	Π_1^*	v_3^*/m·s^{-1}	Er./%
1.17	198862.91	5.212	0.150	168127.04	4.407	0.74	119461.28	3.131	0.032
1.31	196359.59	5.147	0.063	166244.25	4.357	0.39	121751.28	3.191	0.031
1.46	192108.32	5.035	0.093	160134.40	4.200	0.24	112590.18	2.951	0.034
1.60	164216.12	4.304	0.130	139194.31	3.648	0.33	106862.95	2.801	0.036
1.75	163775.84	4.293	0.170	137274.06	3.598	0.33	104189.04	2.731	0.037

Note: Π_1^*, v_1^* represents the data obtained by the Π equation and the empirical formula of v_1; Er. is the abbreviation of Error for the relative error between the data value obtained by the empirical formula and the actual experiment value in Tables 7-10.

2) The results of the second validation analysis. In this verification experiment, each component of the equation needs to be verified, represented by Equation (12).

$$\begin{cases} \dfrac{2.32\times10^{-9}\Pi_2^4-3.42\times10^{-5}\Pi_2^3+0.18\Pi_2^2-333.301\Pi_2-280927}{192108.32}\overset{?}{=}\dfrac{1.54\times10^{-9}\Pi_2^4-2.18\times10^{-6}\Pi_2^3+0.11\Pi_2^2-195.82\Pi_2+179892}{163775.84} \\ \dfrac{-1.80\times10^{11}\Pi_2^4+3.77\times10^{10}\Pi_2^3-2.58\times10^{9}\Pi_3^2+5.24\times10^{7}\Pi_3+514089}{192108.32}\overset{?}{=}\dfrac{-1.31\times10^{11}\Pi_2^4+2.83\times10^{10}\Pi_2^3-1.92\times10^{9}\Pi_3^2+3.20\times10^{7}\Pi_3+767238}{163775.84} \\ \dfrac{5.89\times10^{8}\Pi_4^4-3.11\times10^{8}\Pi_4^3+5.64\times10^{7}\Pi_4^2-4.04\times10^{6}\Pi_4+278602}{192108.32}\overset{?}{=}\dfrac{-1.69\times10^{9}\Pi_4^4+8.55\times10^{8}\Pi_4^3-1.49\times10^{8}\Pi_4^2+1.02\times10^{8}\Pi_4-45732}{163775.84} \\ \dfrac{7.20\times10^{6}\Pi_4^4-4.12\times10^{7}\Pi_5^3+8.86\times10^{7}\Pi_5^2-8.22\times10^{7}\Pi_5+2.89\times10^{7}}{192108.32}\overset{?}{=}\dfrac{-1.76\times10^{7}\Pi_4^4+1.02\times10^{7}\Pi_5^3-6.98\times10^{7}\Pi_5^2+6.87\times10^{7}\Pi_5-2.49\times10^{7}}{186850.31} \end{cases} \tag{12}$$

$\overline{\Pi}_2$, $\overline{\Pi}_3$, $\overline{\Pi}_4$, $\overline{\Pi}_5$ and $\overline{\overline{\Pi}}_4$, $\overline{\overline{\Pi}}_5$ can be obtained from Tables 7-10 by substituting them into Equation (10) to obtain the denominator, and then substituting the Π values of the test into Equation (12) to compare the difference between the data values on the left side and the right side of the equation, the result as listed in Table 12. The results of the second verification show that, for the same independent variable, under the same other experimental conditions, different fixed experimental values are selected to verify the validity of the obtained Π equation. It can be seen that the Π equation does not apply to all conditions, when 1907.61≤ $\rho Q/dX$ ≤5722.83, 0.05≤ d/X ≤0.083, 0.125≤ L/X ≤0.21, 1.17≤ Y_1/X ≤1.46, the relative deviation of the Π equation was less than 10%, which meets the needs of general engineering fields; When d/X ≤4906.42, L/X ≤0.083, Y_1/X ≥1.60, the relative deviation of the Π equation was slightly greater than 10%.

3) The results of the final validation analysis. To verify the conclusion of the secondary verification, other points within the range of the experiment parameters (different from the experiment points required for the establishment of the Π equation) were selected, and additional verification experiments were carried out, as shown in Table 13. It can be seen that when 2437.5≤ $\rho Q/dX$ ≤5298.91, 0.058≤ d/X ≤0.075, 0.067≤ L/X ≤0.183, the relative deviation of the outlet flow rate value of outlet branch pipe 1 predicted by the Π equation from the experimental value is less than 10%, which proves the conclusion of the secondary verification to a certain extent. In conclusion, the Π equation and empirical formula can be used to predict the velocity of outlet branch pipe 1 under the conditions of 1907.61≤ $\rho Q/dX$ ≤5722.83, 0.05≤ d/X ≤0.083, 0.125≤ L/X ≤0.21, 1.17≤ Y_1/X ≤1.46.

Table 12 Results of Π equations effective experiment

Π_2	Relative deviations of substituting $\overline{\overline{\Pi}}_5$ for $\overline{\Pi}_5$ /%			Π_3	Relative deviations of substituting $\overline{\overline{\Pi}}_5$ for $\overline{\Pi}_5$ /%		
	v_1/m·s^{-1}	v_2/m·s^{-1}	v_3/m·s^{-1}		v_1/m·s^{-1}	v_2/m·s^{-1}	v_3/m·s^{-1}
1907.61	6.48	6.15	0.73	0.033	16.68	17.10	8.56
2861.41	0.36	0.24	10.22	0.043	10.69	17.83	9.52
3815.22	2.63	2.15	2.53	0.050	3.44	13.17	6.44
4769.02	2.80	3.38	6.35	0.075	2.63	4.85	2.54
5722.83	6.47	3.26	2.37	0.083	6.67	9.14	1.60

Π_4	Relative deviations of substituting $\overline{\overline{\Pi}}_5$ for $\overline{\Pi}_5$ /%			Relative deviations of substituting $\overline{\overline{\Pi}}_4$ for $\overline{\Pi}_4$ /%					
	v_1/m·s^{-1}	v_2/m·s^{-1}	v_3/m·s^{-1}	Π_5	v_1/m·s^{-1}	Π_5	v_2/m·s^{-1}	Π_5	v_3/m·s^{-1}
0.042	11.00	0.39	3.48	1.17	2.97	0.83	4.19	0.50	5.12
0.083	15.94	12.86	5.91	1.31	2.70	0.94	4.88	0.56	10.21
0.125	4.78	3.17	2.53	1.46	7.45	1.04	1.79	0.63	8.11
0.170	4.77	7.00	1.36	1.60	0.51	1.15	13.12	0.69	5.87
0.210	4.21	5.39	2.71	1.75	0.33	1.25	7.66	0.75	2.59

Table 13 Additional experimental results

Q/m^3·s^{-1}	d/m	L/m	Y_1/m	Y_2/m	Y_3/m	v_1/m·s^{-1}	Er./%	v_2/m·s^{-1}	Er./%	v_3/m·s^{-1}	Er./%
0.023	0.045	0.075	0.875	0.625	0.375	3.10	2.13	2.60	3.69	2.02	0.99
0.032	0.045	0.075	0.875	0.625	0.375	4.22	5.88	3.56	4.86	2.72	1.84
0.041	0.045	0.075	0.875	0.625	0.375	5.24	7.08	4.46	4.98	3.54	6.07
0.050	0.045	0.075	0.875	0.625	0.375	6.60	0.18	5.58	0.63	4.28	3.13
0.036	0.035	0.075	0.875	0.625	0.375	6.21	7.18	5.76	6.39	5.05	10.28
0.036	0.040	0.075	0.875	0.625	0.375	5.31	4.58	4.71	4.54	3.84	7.40
0.036	0.045	0.040	0.875	0.625	0.375	4.86	3.19	4.09	0.76	3.12	3.85
0.036	0.045	0.060	0.875	0.625	0.375	4.83	1.45	4.11	1.20	3.11	3.54
0.036	0.045	0.090	0.875	0.625	0.375	4.86	3.37	4.06	3.74	3.15	4.76
0.036	0.045	0.110	0.875	0.625	0.375	4.93	1.44	4.16	0.34	3.17	1.48
0.036	0.045	0.075	0.840	0.600	0.360	4.9	4.93	4.22	1.87	3.12	1.92
0.036	0.045	0.075	0.910	0.650	0.390	4.93	3.37	4.20	0.07	3.12	9.04

To sum up, combined with the data in Tables 7-10, in the same way, the outlet flow velocity empirical formula of outlet branch pipes 2 and 3 can be further obtained. Among them, the empirical formulas of outlet branch pipe 2 are

$$v_2=(-1.94\times10^{-9}(\rho Q/dX)^4+2.82\times10^{-5}(\rho Q/dX)^3+0.14(\rho Q/dX)^2-267.32\rho Q/dX+227556)\times(-867902.1(d/X)^4+174232.27(d/X)^3-10765.86(d/X)^2+128.64d/X+5.87)\times(-298.69(L/X)^4-198.98(L/X)^3+42.07(L/X)^2-3.25L/X+1.06)\times(-99.09\ (Y/X)^4-404.07$$

$$(Y/X)^3+612.32(Y/X)^2-409.15(Y/X)+102.84)\times\mu/\rho X \quad (13)$$

The empirical formulas of outlet branch pipe 3 are

$$v_3=(-7.89\times10^{-11}(\rho Q/dX)^4+2.54\times10^{-6}(\rho Q/dX)^3-0.021\ (\rho Q/dX)^2+89.66\ \rho Q/dX-53639.5)\times(-1094279.81(d/X)^4+225220.31(d/X)^3-14172.15(d/X)^2+157.43d/X+8.52)\times(-3220.64\ (L/X)^4+1603.18(L/X)^3-270.73\ (L/X)^2+17.7L/X+0.67)\times(-265.77\ (Y/X)^4+706.05(Y/X)^3-697.6(Y/X)^2+302.95(Y/X)-47.6\times\mu/\rho X \quad (14)$$

Combining the three verification data on the velocity of the outlet branch pipes 2 and 3 in Tables 11-13, it can be known that when $1907.61\leq \rho Q/dX \leq 5722.83$, $0.075\leq d/X \leq 0.083$, $0.125\leq L/X \leq 0.210$, $0.83\leq Y_2/X \leq 1.25$, the relative deviation between the velocity value of the outlet branch pipe 2 predicted by the Π equation and the experiment value is less than 10%, the empirical formula can be used for the outlet flow rate prediction of the outlet branch pipe 2, Similarly, it can be seen that when $1907.61\leq \rho Q/dX \leq 5722.83$, $0.033\leq d/X \leq 0.083$, $0.042\leq L/X \leq 0.21$, $0.5\leq Y_3/X \leq 0.75$, the empirical formula can be used to predict the velocity of the outlet branch pipe 3.

In summary, when $1907.61\leq\rho Q/dX\leq 5722.83$, $0.075\leq d/X\leq 0.083$, $0.125\leq L/X\leq 0.210$, $1.17\leq Y_1/X\leq 1.46$ ($0.83\leq Y_2/X\leq 1.25$, $0.60\leq Y_3/X \leq 0.75$), i.e., when $0.018\ m^3/s\leq Q\leq 0.054\ m^3/s$, $0.045\ m\leq d\leq 0.05\ m$, $0.075\ m\leq L \leq 0.125\ m$, $0.7\ m\leq Y_1 \leq 0.875\ m$ ($0.5\ m\leq Y_2 \leq 0.75\ m$, $0.36\ m\leq Y_3\leq 0.45\ m$), the relative deviation between the velocity values of the outlet branch pipes 1, 2, and 3 predicted by the Π equation and the experiment value is less than 10%. The empirical formula can be used for the velocity prediction of outlet branch pipes 1, 2, and 3. The flow prediction of outlet branch pipe 4 can be obtained through the data predicted by outlet branch pipes 1, 2, and 3 in combination with the law of conservation of mass.

5 Conclusions

1) In this study, we analyze the flow mechanism of the airflow from the header into the branch pipe in the multi-branch pipe, and get the main geometric structure factors affecting the air flow of the multi-branch pipe, namely D, L, δ, d, l. Through the mass conservation theorem and the momentum conservation theorem, we theoretically determine that ρ, μ, and Q are the main factors affecting the airflow parameters of the outlet branch pipe of the multi-branch pipe; and through Fluent simulation software, combined with the simulation experiment results, it is clear that the difference of local resistance loss in the outlet branch pipe of multi-branch pipe is the main reason for the difference of air parameters in the outlet branch pipe.

2) The empirical formula of airflow parameter values of outlet branch pipe of multi-branch pipe was established by using the method of dimensional analysis, and the applicable range of the empirical formula was determined by Π theorem; in the range of $0.018\ m^3/s\leq Q\leq 0.054\ m^3/s$, $0.045\ m\leq d\leq 0.05\ m$, $0.075\ m\leq L \leq 0.125\ m$, $0.7\ m\leq Y_1\leq 0.875\ m$ ($0.5\ m\leq Y_2\leq 0.75\ m$, $0.36\ m\leq Y_3\leq 0.45\ m$), the prediction accuracy of the empirical formula can be controlled within the range of 10%, which meets the general engineering accuracy requirements. The established empirical formula has certain significance for the pipeline selection and design optimization of similar models.

Acknowledgements

This work was financially supported by the National Natural Science Foundation of China (Grant No. 52175228), the earmarked fund for the National Key Research and Development program of China (Grant No. 2021YFD2000403), the scientific research fund for the Guangdong Laboratory for Lingnan Modern Agriculture (Grant No. NZ2021039), the earmarked fund for CARS-01, and the earmarked fund for the Guangdong Province Key Field Research and Development Program (Grant No. 2020B020210007).

[References]

[1] Robert L, Pigford, Muhammad A, Yvon D M. Flow distribution in piping manifolds. Ind Eng Chem Fundam, 1983; 22(4): 463–471.

[2] Song P F, Yang L R. Research and design on flow characteristics of Single-phase multi-branch parallel pipeline. Petroleum Refinery Engineering, 2020; 50(3): 42–47. (in Chinese)

[3] Łukasz A, Janusz W. Thermal performance of multi-pipe earth-to-air heat exchangers considering the non-uniform distribution of air between parallel pipes. Renewable Energy, 2018; (88): 101896. doi: 10.1016/j.geothermics.2020.101896.

[4] Foo K, Roy M, Klaus A H. Numerical assessment of pulsatile flow through diverging tees with a sharp and round-edge junction. Int J Heat and Fluid Flow, 2019; 76: 1–13.

[5] Dong J, Ben X H. CFD analysis of a novel modular manifold with multi-stage Channels for uniform air distribution in a fuel cell stack. Applied Thermal Engineering, 2017; 124: 286–293.

[6] Mohammad A Z, Elham O A. Study of the flow distribution in Parallel micro-channels with a triangular manifold. J Braz Soc Mech Sci, 2019; 42(1): 46. doi: 10.1007/s40430-019-2140-x.

[7] Ikeda A, Yoshida T, Shirota M, Takei M. Method of the non-split application of fertilizer to rice "Kosihikari" on pneumatic direct seeding culture on submerged paddy filed. Res Bull Aichi Agric Res Ctr, 2003; 35: 23–29.

[8] Zhang G Q, Christopher C, Thomas B, Lee I-B, Kacira M. Computational fluid dynamics (CFD) research and application in agricultural and biological engineering. Comput Electron Agri, 2018; 14: 1–2.

[9] Xing H, Zang Y, Wang Z M, Luo X W, Pei J, He S Y, et al. Design and parameter optimization of rice pneumatic seeding metering device with adjustable seeding rate. Transactions of the CSAE, 2018; 35(4): 20–28. (in Chinese)

[10] Salavat M, Ildar B, Zinnur R, Ramil L, Elmas N. Numerical simulation of two-phase "Air-Seed" flow in the distribution system of the grain seeder. Comput Electron Agri, 2020; 168: 105151. doi: 10.1016/j.compag.2019.105151.

[11] Liao Q X, Yang S, Liao Y T, Cong J H. Modeling for performance and parameters of pneumatic seed-metering system of precision planter for rapeseed. Transactions of the CSAE, 2013; 29(17): 9–15. (in Chinese)

[12] Yin X W, Yang L, Zhang D, Cui T, Han D, Zhang T, et al. Design and experiment of balance and low-loss air allotter in air pressure maize precision planter. Transactions of the CSAE, 2016; 32(19): 9–17. (in Chinese)

[13] Yasuhiko S, Seiichi I, Ikuma E, Hideyuki H, Kazuo H. development of pneumatic direct seeding system for submerged paddy field (Part 1)-Basic study on the development of seeding system. J Jpn Agri Machinery Soc, 1996; 58(3): 69–76.

[14] Tadashi C, Masami F, Masaaki O, Osamu M. Development of air-assisted strip seeding for direct seeding in flooded paddy fields: Seeding machine and effect of air assistance. Jpn J Farm Work Res, 2009; 44(4): 211–218.

[15] Nguyen T H, Tadashi C, Seishu T, Ngo T H. Application of a similarity measure using fuzzy sets to select the optimal plan for an air-assisted rice seeder. Applied Science, 2021; 11(6715): 1–15.

[16] Masami F, Tadashi C, Yukiharu S, Takayuki T, Masahiro S, Hisashi H. Developing direct seeding cultivation using an air-assisted strip seeder. Jpn Agric Res Q, 2015; 49(3): 227–233.

[17] Hassan J M, Abdulwahhab A, Kamil B K. Flow distribution in manifolds. J Eng Sustain Dev, 2008; 12(4): 159–176.

[18] Jimmy C K T, Ephraim M S, John P A. Geometric strategies for attainment of identical outflows through all of the exits ports of a distribution manifold in a manifold system. Applied Thermal Engineering, 2009; 29(17-18): 3552–3560.

[19] Shu C X, Wei Y P, Liao Y T, Lei X L, Li Z D, Wang D, et al. Influence of air blower parameters of pneumatic seed-metering system for rapeseed

on negative pressure characteristics and air blower selection. Transactions of the CSAE, 2016; 32(10): 26–33. (in Chinese)

[20] Qin L, Zhou F, Yang J X, Wu R Z, Lu L. Numerical research on flow distribution and pressure loss of multi-branch pipeline based on confluence and distribution. J South China Univ Techno: Nat Sci Ed, 2021; 49(9): 109–119. (in Chinese)

[21] Jiang Y. Proper formulation of π-equation and a comparison with regressive orthogonal rotating experimental design. Transactions of the CSAE, 1996; 12(3): 7–11. (in Chinese)

[22] Jiang Y. Verification of the theory for a sphere settling in fluid with resistance in different ranges by experiment of π-testing Design. Transactions of the CSAE, 1996; 12(3): 12–15. (in Chinese)

[23] Jiang Y, Tu C, Liu D, Jiang E C. Examination of function of π-equation's prediction via experiment of settling time of a sphere in a fluid. Transactions of the CSAE, 1996; 12(3): 1–6. (in Chinese)

[24] Zhang Z G, Jiang Y Y, Zhang M, Shen D C. Experimental study on rapeseed extrusion cooking using dimensional analysis. Transactions of the CSAE, 2007; 23(7): 247–252. (in Chinese)

[25] Sivasankaran S, Hany R A, Abdulaziz S A, Mohammad S. Mathematical modeling (buckingham's π theorem) and optimization technique on mechanically alloyed nanocomposite materials. Int J Eng Adv Technol, 2020; 4(9): 1915–1921.

[26] Li J H, Lai Q H, Su W, Xie Y R, Zhang Z G. Research on the influence of the suction force on spherical particles in suction flow. Powder Technology, 2021; 393(9): 824–836.

[27] André Z S, Sérgio L J, Sávio S V V. The effect of the volumetric flow rate and endotracheal tube diameter on the pressure distribution in human airways. Med Eng Phys, 2021; 92: 71–79.

[28] Han D D, Zhang D X, Jing H R, Yang L, Cui T, Ding Y Q, et al. DEM-CFD coupling simulation and optimization of an inside-filling air-blowing maize precision seed-metering device. Comput Electron Agri, 2018; 150: 426–438.

[29] Zheng W H, Jiang Y, Ma X, Qi L. Development of a liquid-jet nozzle for fertilizer injection in paddy fields using CFD. Comput Electron Agri, 2019; 167: 105061. doi: 10.1016/j.compag.2019.105061.

[30] Xing H, Wang Z M, Luo X W, Cao X M, Liu C B, Zang Y. General structure design and field experiment of pneumatic rice direct-seeder. Int J Agri Bio Eng, 2021; 10(6): 31–42.

[31] Bajura R A. A Model for Flow Distribution in Manifolds. J. Eng. Power, 1971; 93(1): 7–13.

[32] Xing H, Wang Z M, Luo X W, Zang Y, He S Y, Peng X, et al. Design and experimental analysis of rice pneumatic seeder with adjustable rate. Int J Agri Bio Eng, 2021; 14(4): 113–122.

[33] Xing H, Wang Z M, Luo X W, He S Y, Zang Y. Mechanism modeling and experimental analysis of seed throwing with rice pneumatic seed metering device with adjustable seeding rate. Comput Electron Agri, 2020; 178: 105697. doi: 10.1016/j.compag.2020.105697.

[34] Xing H, Wang Z M, Luo X W, Cao X M, Liu C B, Zang Y. General structure design and field experiment of pneumatic rice direct-seeder. Int J Agric & Biol Eng, 2017; 10(6): 31–42.